PHYSICAL REVIEW D **81,** 034508 (2010)

Quarkonium mass splittings in three-flavor lattice QCD

T. Burch,[1] C. DeTar,[1] M. Di Pierro,[2] A. X. El-Khadra,[3] E. D. Freeland,[4] Steven Gottlieb,[5,6] A. S. Kronfeld,[7] L. Levkova,[1] P. B. Mackenzie,[7] and J. N. Simone[7]

(Fermilab Lattice and MILC Collaborations)

[1]*Department of Physics, University of Utah, Salt Lake City, Utah, USA*
[2]*School of Computing, DePaul University, Chicago, Illinois, USA*
[3]*Physics Department, University of Illinois, Urbana, Illinois, USA*
[4]*Department of Physics, Washington University, St. Louis, Missouri, USA*
[5]*Department of Physics, Indiana University, Bloomington, Indiana, USA*
[6]*National Center for Supercomputing Applications, University of Illinois, Urbana, Illinois, USA*
[7]*Fermi National Accelerator Laboratory, Batavia, Illinois, USA*
(Received 17 December 2009; published 12 February 2010)

We report on calculations of the charmonium and bottomonium spectrum in lattice QCD. We use ensembles of gauge fields with three flavors of sea quarks, simulated with the asqtad improved action for staggered fermions. For the heavy quarks we employ the Fermilab interpretation of the clover action for Wilson fermions. These calculations provide a test of lattice QCD, including the theory of discretization errors for heavy quarks. We provide, therefore, a careful discussion of the results in light of the heavy-quark effective Lagrangian. By and large, we find that the computed results are in agreement with experiment, once parametric and discretization errors are taken into account.

DOI: 10.1103/PhysRevD.81.034508 PACS numbers: 12.38.Gc, 14.40.Pq

I. INTRODUCTION

Quarkonium plays an important role in the application of QCD to hadronic physics. Early calculations of charmonium based on potential models gave strong support to the interpretation of these states as bound states of a new heavy quark [1,2]. Although physically the charmonium state is analogous to positronium, its historical role as a model system of QCD proved to be analogous to that of the hydrogen atom in quantum mechanics. The charmonium spectrum provided a simple example of how QCD works, made even more compelling with the subsequent observation of the bottomonium states.

Although the analysis of the quarkonium spectrum based on potential models is a significant triumph of QCD, an *ab initio* calculation based on lattice QCD, an approach that can simultaneously deal with light quarks would be even more satisfying. However, in lattice QCD, the continuum limit requires that am approaches zero, where a is the lattice spacing and m is the mass of the state. Quarkonium states and their constituent quarks are so heavy that it is often impractical to use so small a lattice spacing that am is small. Both lattice nonrelativistic QCD (NRQCD) [3,4] and the Fermilab action [5] have been developed to treat heavy quarks in lattice gauge theory. Thus, the successful calculation of the spectrum of charmonium and bottomonium becomes a significant test of these techniques.

This paper describes the current state of the quarkonium spectrum based on the Fermilab approach to heavy quarks, using gauge configurations provided by the MILC Collaboration [6] that incorporate the effects of three light quarks: up, down, and strange. We have been studying the quarkonium spectrum using this formalism for some time [7], starting on ensembles with two flavors of sea quark [8], and new ensembles of configurations have become available during the course of the project. In this paper, we report on results with four lattice spacings from $a \approx 0.18$ fm to ≈ 0.09 fm. We do not yet consider this work a definitive calculation using our approach. Results from two finer lattice spacings should become available in the future. As we detail below, the tuning of the bare valence heavy-quark masses, via the heavy-light meson spectrum [9], is not yet precise enough to give satisfactory answers to all the questions that have arisen. In the future, we expect to have better control of the heavy-quark masses. Nevertheless, already we can successfully reproduce important features of the quarkonium spectrum, and we consider this another important test bed in which to assess the errors that arise from our treatment of the heavy quarks. Knowledge of these errors is also important for calculations of properties of heavy-light mesons, for example, those pertaining to semileptonic decays [10], leptonic decays [11], and B-$\bar{B}$ mixing [12], as well as the heavy-light spectrum [9].

Prior lattice QCD work on quarkonium with different sea-quark content has been reviewed by Bali [13]. More recently, Dudek and collaborators have used the quenched approximation to explore decays [14], radiative transitions [15], and the excited-state spectrum [16] of charmonium. Meinel has used lattice NRQCD to compute the bottomo-

nium spectrum at one lattice spacing on four ensembles with $2+1$ domain-wall sea quarks [17]. The HPQCD Collaboration has calculated the quarkonium spectrum on many of the same MILC ensembles used in our work, using lattice NRQCD for bottomonium [18,19], and using highly improved staggered quarks (HISQ) for charmonium [20]. Lattice NRQCD is not very accurate for charmonium, and HISQ requires very small lattice spacings for b quarks [21]. An advantage of the Fermilab method is that it allows the same treatment for both the charmed and bottom quarks. Predictions of the $c\bar{b}$ spectrum have also been made, for the pseudoscalar B_c using NRQCD b quarks and the charmed quark propagators from this project [22], and also for the vector B_c^* using NRQCD b quarks and HISQ charmed quarks [23].

The plan of this paper is as follows. In Sec. II, we describe our methodology, explaining the actions used for gluons, light sea quarks, and the heavy valence quarks. We describe, in detail, how to use the heavy-quark effective Lagrangian to understand heavy-quark discretization errors in quarkonium masses. We also discuss the construction of the hadronic correlators and how they are fit to determine meson masses. Several broad issues inform the uncertainties (statistical and systematic), and they are discussed in Sec. III. In Sec. IV, we show our results for the splittings between various states or combinations of states. Where possible, we have organized the presentation of the mass splittings around individual terms in the heavy-quark effective action, which clarifies the approach to the continuum limit at available lattice spacings. Section V contains our conclusions and suggestions on ways to improve on this calculation.

II. METHODOLOGY

In this section, we collect several sets of information needed to understand the results that follow. Section II A defines the notation for different quarkonium states and splittings. Then we provide details of the lattice gauge configurations that we have used in Sec. II B. Next, in Sec. II C, we review the Fermilab method, discussing in detail how it can be understood via an effective Lagrangian. This discussion provides a link between the lattice fermion action and the computed mass splittings; an important theme in this paper is to scrutinize our numerical results according to these theoretical expectations. Last, we explain how we form correlation functions in Sec. II D, and how we fit them to obtain masses in Sec. II E.

A. Notation

In this paper, we use two notations for hadrons and their masses, both the standard names from the Particle Data Group [24] and the spectroscopic notation $n^{2S+1}L_J$, where S, L, and J are the spin, orbital, and total angular momentum, respectively, of the nth radial excitation. As usual, $L = 0, 1, 2, \ldots$ are denoted $S, P, D, \ldots$.

It is often convenient to discuss spin-averaged masses (and mass splittings), which we indicate with a horizontal line, such as $\overline{1S}$ or $\overline{1^3P}$. In particular,

$$M(\overline{1S}) = \frac{1}{4}(M_{\eta_c} + 3M_{J/\psi}), \tag{2.1}$$

$$M(\overline{1^3P}) = \frac{1}{9}(M_{\chi_{c0}} + 3M_{\chi_{c1}} + 5M_{\chi_{c2}}), \tag{2.2}$$

using charmonium for illustration. For brevity we usually write $\overline{1P}$ for $\overline{1^3P}$. These spin-averages are sensitive to the leading term in a nonrelativistic expansion. Note that the $\overline{1P}$ and 1^1P_1 (also denoted h_c and h_b) levels are nearly the same in nature, which can be explained by the spin-spin interaction's short range—$\delta(\boldsymbol{r})$ in the context of potential models [2].

Complementary to the spin-averaged masses are spin-splittings that hone in on spin-dependent corrections [25,26]. Below, we examine the hyperfine splittings (HFS)

$$M(nS_{\mathrm{HFS}}) = M_{J/\psi} - M_{\eta_c}, \tag{2.3}$$

using charmonium $1S$ notation on the right-hand side. For the P states two combinations are of interest:

$$M(nP_{\text{spin-orbit}}) = \frac{1}{9}(5M_{\chi_{c2}} - 2M_{\chi_{c0}} - 3M_{\chi_{c1}}), \tag{2.4}$$

$$M(nP_{\text{tensor}}) = \frac{1}{9}(3M_{\chi_{c1}} - M_{\chi_{c2}} - 2M_{\chi_{c0}}), \tag{2.5}$$

again using charmonium $1S$ notation on the right-hand side. $M(nS_{\mathrm{HFS}})$ and $M(nP_{\text{tensor}})$ are sensitive to spin-spin interactions, and $M(nP_{\text{spin-orbit}})$ to spin-orbit interactions.

B. Configuration details

These calculations have been carried out on lattice gauge configurations provided by the MILC Collaboration [6], listed in Table I. They were generated via the R algorithm [27] with the one-loop Symanzik-improved Lüscher-Weisz gluon action [28] combined with $2+1$ flavors of sea quarks simulated with the asqtad action [29]. The n_f-dependent part of the one-loop couplings [30] became available only after the ensembles were generated. We have used ensembles at four lattice spacings: $a \approx 0.18$, 0.15, 0.12, and 0.09 fm (also called in the text "extra-coarse," "medium-coarse," "coarse," and "fine" ensembles, respectively). The first four columns of Table I list the parameters of these ensembles, including the masses of the sea quarks, denoting the pair as am_l/am_s. The lattice scale of each ensemble with different sea-quark masses was kept approximately fixed using the length r_1 [31,32] from the static quark potential. The absolute scale from the Υ $2S$-$1S$ splitting was determined on most of our ensembles by the HPQCD Collaboration [18,19]. Details on the r_1 determinations can be found in review of other work on the MILC ensembles [33]. Combining this deter-

TABLE I. Run parameters and configuration numbers for the ensembles used to study charmonium and bottomonium η, J/ψ, Υ, h, χ_0, and χ_1 states with relativistic operators, and h and all χ_J states with nonrelativistic operators. The labels a and b are used to distinguish between the two runs with the same $\beta = 6.76$ but different am_l/am_s.

				Relativistic				Nonrelativistic			
a (fm)	β	am_l/am_s	$N_s^3 \times N_t$	κ_c	$N_{\rm conf}^c$	κ_b	$N_{\rm conf}^b$	κ_c	$N_{\rm conf}^c$	κ_b	$N_{\rm conf}^b$
≈ 0.18	6.503	0.0492/0.082	$16^3 \times 48$	0.120	401	⋯		0.120	400	⋯	
	6.485	0.0328/0.082	$16^3 \times 48$	0.120	331			0.120	501		
	6.467	0.0164/0.082	$16^3 \times 48$	0.120	645			0.120	647		
	6.458	0.0082/0.082	$16^3 \times 48$	0.120	400			0.120	601		
≈ 0.15	6.600	0.0290/0.0484	$16^3 \times 48$	⋯		⋯		0.122	580	0.076	595
	6.586	0.0194/0.0484	$16^3 \times 48$	0.122	631	0.076	631	0.122	580	0.076	595
	6.572	0.0097/0.0484	$16^3 \times 48$	0.122	631	0.076	631	0.122	629	0.076	631
	6.566	0.00484/0.0484	$20^3 \times 48$	⋯		⋯		0.122	601	0.076	600
≈ 0.12	6.81	0.03/0.05	$20^3 \times 64$	0.122	549	0.086	549	⋯		⋯	
	6.79	0.02/0.05	$20^3 \times 64$	0.122	460	0.086	460				
	6.76, a	0.01/0.05	$20^3 \times 64$	0.122	593	0.086	539				
	6.76, b	0.007/0.05	$20^3 \times 64$	0.122	403	⋯					
≈ 0.09	7.11	0.0124/0.031	$28^3 \times 96$	0.127	517	0.0923	517	0.127	518	0.0923	510
	7.09	0.0062/0.031	$28^3 \times 96$	0.127	557	0.0923	557	0.127	557	0.0923	557
	7.08	0.0031/0.031	$40^3 \times 96$	0.127	504	0.0923	504	0.127	504	0.0923	504

mination with more recent work [34,35], leads us to take the range $r_1 = 0.318^{+0.000}_{-0.007}$ fm in this paper.

C. Heavy-quark formulation

In this work, the charmed and bottom quarks are simulated with the Fermilab action [5]

$$\begin{aligned} S = &\sum_n \bar\psi_n \psi_n - \kappa \sum_n [\bar\psi_n (1-\gamma_4) U_{n,4} \psi_{n+\hat 4} \\ &+ \bar\psi_{n+\hat 4}(1+\gamma_4) U^\dagger_{n,4} \psi_n] - \kappa\zeta \sum_{n,i} [\bar\psi_n (r_s - \gamma_i) U_{n,i} \psi_{n+\hat\imath} \\ &+ \bar\psi_{n+\hat\imath}(r_s+\gamma_i) U^\dagger_{n,i} \psi_n] - c_B \kappa\zeta \sum_n \bar\psi_n i\boldsymbol{\Sigma}\cdot\boldsymbol{B}_n \psi_n \\ &- c_E \kappa\zeta \sum_n \bar\psi_n \boldsymbol{\alpha}\cdot\boldsymbol{E}_n \psi_n, \end{aligned} \tag{2.6}$$

where U denotes the gluon field, and ψ and $\bar\psi$ denote the quark and antiquark fields. The clover definitions of the chromomagnetic and chromoelectric fields $\boldsymbol{B}$ and $\boldsymbol{E}$ are standard and given, for example, in Ref. [5]. When $\zeta = r_s = 1$ and $c_B = c_E = 0$, S reduces to the Wilson action [36]; when $\zeta = r_s = 1$ and $c_B = c_E = c_{\rm SW}$, it reduces to the Sheikholeslami-Wohlert action [37]. The relation between the hopping parameter κ and the bare mass is

$$m_0 a = \frac{1}{2\kappa} - 1 - 3 r_s \zeta \tag{2.7}$$

in four space-time dimensions.

To motivate our choices of the input parameters κ, ζ, r_s, c_B, and c_E, let us review the nonrelativistic interpretation of Wilson fermions [5]. The pole energy of a single quark of spatial momentum $\boldsymbol{p}$ is

$$E(\boldsymbol{p}) = m_1 + \frac{\boldsymbol{p}^2}{2m_2} + O(p^4), \tag{2.8}$$

where the quark rest mass m_1 and the kinetic mass m_2 are defined at all orders of perturbation theory via the self energy [38]. At the tree level,

$$m_1 = a^{-1} \ln(1 + m_0 a), \tag{2.9}$$

$$\frac{1}{m_2} = \frac{2\zeta^2}{m_0(2+m_0 a)} + \frac{a r_s \zeta}{1+m_0 a}. \tag{2.10}$$

In general, $m_1 \neq m_2$ unless $m_0 a \ll 1$; for charmed and bottom quarks on the ensembles listed in Table I one has $m_{0c} a \lesssim 1$, $m_{0b} a \gtrsim 1$. One could tune ζ so that $m_2 = m_1$, and we shall revisit that strategy below.

Equation (2.8) is the simplest example of a nonrelativistic interpretation of physical quantities computed with the action in Eq. (2.6). This is justified, because in quarkonium the relative momentum of the heavy quarks is small compared with the heavy-quark mass. This is the basis of the phenomenological success of potential models, which yield estimates of the relative velocity and, equivalently, internal momentum. For charmonium

$$v \approx 0.55, \qquad p \approx 840 \text{ MeV}, \tag{2.11}$$

and for bottomonium

$$v \approx 0.31, \qquad p \approx 1475 \text{ MeV}. \tag{2.12}$$

For both systems the typical kinetic energy is 450 MeV, as seen, for example, in the $\overline{1P}$-$\overline{1S}$ splitting. The kinetic energies $\frac{1}{2} m_2 v^2$ are small on our lattices, and the momenta $m_2 v$ are marginally small (especially for bottomonium).

The nonrelativistic interpretation can be extended beyond the tree level and to higher order in the nonrelativistic expansion using effective field theories. This has been pursued in detail emphasizing heavy-light hadrons [39–41], and here we explain the ideas in the context of quarkonium. As in the Symanzik effective theory, one introduces a continuum effective Lagrangian, but here it is an effective Lagrangian valid for heavy quarks. With quarkonium, the appropriate power-counting rule for the effective Lagrangian is that of nonrelativistic QED [42] and nonrelativistic QCD [3,4,43]. So one has

$$S \doteq -\sum_s \int d^4x \mathcal{L}^{(s)}_{\mathrm{HQ}}, \tag{2.13}$$

where s counts the powers of velocity. Here $\doteq$ means that the lattice gauge theory on the left-hand side, defined in our case by Eq. (2.6), is given an effective description by the right-hand side. The first several terms of the effective Lagrangian are

$$\begin{aligned}\mathcal{L}^{(2)}_{\mathrm{HQ}} = & -\bar{h}^{(+)}(D_4 + m_1)h^{(+)} + \frac{\bar{h}^{(+)}\boldsymbol{D}^2 h^{(+)}}{2m_2} \\ & - \bar{h}^{(-)}(D_4 + m_1)h^{(-)} + \frac{\bar{h}^{(-)}\boldsymbol{D}^2 h^{(-)}}{2m_2},\end{aligned} \tag{2.14}$$

$$\begin{aligned}\mathcal{L}^{(4)}_{\mathrm{HQ}} = & \frac{\bar{h}^{(+)} i\boldsymbol{\sigma}\cdot\boldsymbol{B} h^{(+)}}{2m_B} + \frac{\bar{h}^{(+)} i\boldsymbol{\sigma}\cdot(\boldsymbol{D}\times\boldsymbol{E}) h^{(+)}}{8m_E^2} \\ & + \frac{\bar{h}^{(+)}(\boldsymbol{D}\cdot\boldsymbol{E}) h^{(+)}}{8m_{E'}^2} + \frac{\bar{h}^{(+)}(\boldsymbol{D}^2)^2 h^{(+)}}{8m_4^3} \\ & + \frac{1}{6}a^3 w_4 \bar{h}^{(+)} D_i^4 h^{(+)} + \frac{\bar{h}^{(-)} i\boldsymbol{\sigma}\cdot\boldsymbol{B} h^{(-)}}{2m_B} \\ & - \frac{\bar{h}^{(-)} i\boldsymbol{\sigma}\cdot(\boldsymbol{D}\times\boldsymbol{E}) h^{(-)}}{8m_E^2} - \frac{\bar{h}^{(-)}(\boldsymbol{D}\cdot\boldsymbol{E}) h^{(-)}}{8m_{E'}^2} \\ & + \frac{\bar{h}^{(-)}(\boldsymbol{D}^2)^2 h^{(-)}}{8m_4^3} + \frac{1}{6}a^3 w_4 \bar{h}^{(-)} D_i^4 h^{(-)},\end{aligned} \tag{2.15}$$

where $h^{(+)}$ is a two-component field describing the quark, and $h^{(-)}$ is a two-component field describing the antiquark. The short-distance coefficients m_1, m_2^{-1}, m_B^{-1}, m_E^{-2}, $m_{E'}^{-2}$, m_4^{-3}, and w_4 depend on the bare quark masses, the bare gauge coupling, and all other couplings of the (improved) lattice action. The terms in $\mathcal{L}^{(s)}_{\mathrm{HQ}}$ scale with the heavy quark's velocity as v^s, with the rules [4] $\boldsymbol{D} \sim m_2 v$, $\boldsymbol{E} \sim m_2^2 v^3$, and $\boldsymbol{B} \sim m_2^2 v^4$. In particular, the nonrelativistic kinetic energy, $\boldsymbol{D}^2/2m_2 \sim \frac{1}{2}m_2 v^2$, is an essential part of quarkonium dynamics, which is why m_2 appears with v in the power counting. The short-distance coefficients m_B^{-1}, m_E^{-2}, etc., can be expanded in perturbation theory, with $\alpha_s \sim v$ [4]. We have put the rest mass $m_1\bar{h}^{(\pm)}h^{(\pm)}$ and temporal kinetic energy $\bar{h}^{(\pm)}D_4 h^{(\pm)}$ into $\mathcal{L}^{(2)}_{\mathrm{HQ}}$, because by the equation of motion $D_4 + m_1 \sim \boldsymbol{D}^2/2m_2 \sim \frac{1}{2}m_2 v^2$. The next set of terms, $\mathcal{L}^{(6)}_{\mathrm{HQ}}$, are not written out, because they are numerous yet merely describe subleading contributions to the splittings examined below.

One would like to adjust κ, ζ, r_s, c_B, and c_E so that the lattice gauge theory matches continuum QCD with controllable uncertainty. One would also like to reduce the number of input parameters as much as possible, to make the simulation easier to carry out. The coupling r_s is redundant: any choice is allowed as long as the doubling problem is solved. We take

$$r_s = 1. \tag{2.16}$$

To derive tuning criteria for the others, one refers to the NRQCD description of continuum QCD, which takes the same form as Eqs. (2.14) and (2.15), but with the following substitutions:

$$m_1 \mapsto m, \tag{2.17}$$

$$m_2 \mapsto m, \tag{2.18}$$

$$\frac{1}{m_B} \mapsto \frac{Z_B}{m}, \tag{2.19}$$

$$\frac{1}{m_E^2} \mapsto \frac{Z_E}{m^2}, \tag{2.20}$$

$$\frac{1}{m_{E'}^2} \mapsto \frac{Z_{E'}}{m^2}, \tag{2.21}$$

$$\frac{1}{m_4^3} \mapsto \frac{Z_4}{m^3}, \tag{2.22}$$

$$w_4 \mapsto 0, \tag{2.23}$$

where the last is a consequence of Lorentz invariance, as is the exact equality of the rest and kinetic masses. The matching factors Z_i are unity at the tree level and have a perturbative expansion. To bring the lattice field theory in line with continuum QCD, one must then simply adjust the lattice couplings so that the lattice quantities on the left in (2.17), (2.18), (2.19), (2.20), (2.21), (2.22), and (2.23) become, to some accuracy, the continuum quantities on the right. In principle, this matching could be carried out nonperturbatively [44], although we do not pursue that strategy here.

If one restricts one's attention to mass splittings and matrix elements, it is not necessary to adjust a coupling to tune m_1. The operators $\bar{h}^{(\pm)}h^{(\pm)}$ are number operators, commuting with everything else in the Hamiltonian [39]. It is therefore acceptable to tolerate a large discretization error in the rest mass and, consequently, one does not need to adjust ζ. We take

$$\zeta = 1. \tag{2.24}$$

To obtain the correct dynamics, one must adjust κ so that the rest of $\mathcal{L}^{(2)}_{\rm HQ}$ is correctly tuned. In other words, one must identify the kinetic quark mass m_2 with the physical quark mass.

The adjustment of c_B stems from a concrete realization of (2.19). At the tree level

$$\frac{1}{m_B} = \frac{2\zeta^2}{m_0(2+m_0a)} + \frac{ac_B\zeta}{1+m_0a}, \tag{2.25}$$

so to ensure $m_B = m_2$ (as desired at the tree level where $Z_B = 1$), one needs $c_B = r_s$. In practice, we take [recalling Eq. (2.16)]

$$c_B = u_0^{-3} \tag{2.26}$$

to account for tadpole diagrams at higher orders in perturbation theory [45]. On the coarse ensembles, we set u_0 from the Landau link; on the other ensembles, we set it from the plaquette.

In principle, the adjustment of c_E should stem from (2.20). These simulations have been carried out, however, in concert with calculations of heavy-light masses [9], for which the adjustment of c_E is a subleading effect [39,46]. Thus, we have taken

$$c_E = c_B. \tag{2.27}$$

Using formulas in Ref. [47], we can estimate the error stemming from $1/m_E^2$, finding a tree-level mismatch of

$$\frac{1}{4m_E^2} - \frac{1}{4m_2^2} = \frac{a^2}{(2+m_0a)(1+m_0a)} - \frac{a^2}{4(1+m_0a)^2}, \tag{2.28}$$

where the right-hand side holds for $\zeta = r_s = c_B = c_E = 1$. At the tree level $m_E = m_{E'}$, so the same error is made in the Darwin terms $\bar{h}^{(\pm)}\boldsymbol{D}\cdot\boldsymbol{E}h^{(\pm)}$.

An advantage of using Eqs. (2.13), (2.14), and (2.15) to describe our lattice calculation is that it clarifies which parameters in S play a key role in various splittings defined in Sec. II A. The spin-averaged masses receive energy (beyond $2m_1$) from the balance between the kinetic energies $\bar{h}^{(\pm)}\boldsymbol{D}^2h^{(\pm)}$ and the exchange of temporal gluons between $\bar{h}^{(+)}A_4h^{(+)}$ and $\bar{h}^{(-)}A_4h^{(-)}$. As discussed above, they are sensitive to m_2, motivating the tuning of κ (and the fixed choice for ζ.) The hyperfine splittings $M(nS_{\rm HFS})$ arise from exchange of spatial gluons between $\bar{h}^{(+)}i\boldsymbol{\sigma}\cdot\boldsymbol{B}h^{(+)}$ and $\bar{h}^{(-)}i\boldsymbol{\sigma}\cdot\boldsymbol{B}h^{(-)}$. Hence they are proportional to $1/m_B^2$ and, drilling further back to S, sensitive to the coupling c_B. The same line of dependency holds for the tensor splittings $M(nP_{\rm tensor})$. Similarly, the spin-orbit parts of the χ_{cJ} and χ_{bJ} levels arise from exchange of a temporal gluon between $\bar{h}^{(\pm)}i\boldsymbol{\sigma}\cdot(\boldsymbol{D}\times\boldsymbol{E})h^{(\pm)}$ and $\bar{h}^{(\mp)}A_4h^{(\mp)}$. Hence they are proportional to $1/m_E^2$ and, referring back to S, sensitive to c_E.

With the tree-level adjustment of c_B, the hyperfine splittings should be expected to have errors of order $\alpha_s m v^4$ from radiative corrections to m_B^{-1} [relative error: $O(\alpha_s) \sim O(v)$], and of order v^6 from the terms $\bar{h}^{(\pm)}\{\boldsymbol{D}^2, i\boldsymbol{\sigma}\cdot\boldsymbol{B}\}h^{(\pm)}$ in $\mathcal{L}^{(6)}_{\rm HQ}$ [relative error: $O(v^2)$]. Similarly, with $c_E = c_B$, we expect leading errors of order $a^2m^3v^4$ in the spin-orbit part of the χ splittings [relative error: $O(m^2a^2)$], as well as radiative corrections to m_E^{-2} [relative error: again $O(\alpha_s) \sim O(v)$]. On the MILC ensembles both relative errors are expected to be a few to several percent [47] and, perhaps counterintuitively, smaller for bottomonium than charmonium [47].

The lattice action in Eq. (2.6) does not contain parameters to tune the two terms proportional to p^4 in Eq. (2.15). The mismatches

$$\frac{1}{8m_4^3} - \frac{1}{8m_2^3} = \frac{a^2}{2m_0(2+m_0a)^2(1+m_0a)} + \frac{a^2(1+4m_0a)}{4m_0(2+m_0a)(1+m_0a)^2} + \frac{m_0a^4}{8(1+m_0a)^3} \tag{2.29}$$

and

$$a^3w_4 = \frac{2a^2}{m_0(2+m_0a)} + \frac{a^3}{4(1+m_0a)} \tag{2.30}$$

(given again for $\zeta = r_s = c_B = c_E = 1$) cause errors of order $a^2m^3v^4$ in the spin-averaged splittings. The relative errors, $O(m^2a^2)$, are again expected to be a few to several percent, but in this case larger for bottomonium than for charmonium [47]. For plots of the a dependence of discretization effects caused by Eqs. (2.28), (2.29), and (2.30), see Figs. 2 and 3 of Ref. [47].

To tune κ nonperturbatively, one adjusts it so that a hadron mass agrees with the experimentally measured value. Let us define M_1 and M_2 for a hadron analogously to Eq. (2.8).[1] From the effective Lagrangian description for quarkonium, Eqs. (2.13), (2.14), and (2.15), it follows that

$$M_1 = 2m_1 + B_1, \tag{2.31}$$

$$M_2 = 2m_2 + B_2, \tag{2.32}$$

where the binding energy B_1 is determined by terms of order v^2 and higher, but B_2 by terms of order v^4 and higher [48]. In the splittings of rest masses, m_1 drops out, so we can obtain well-tuned results for B_1 (and their differences) by adjusting κ so that m_2 corresponds to a physical quark. That suggests tuning κ so that, say, $M_2(\overline{1S})$ agrees with experiment. The spin average is useful, because it elimi-

[1] In this paper, we use $m_1, m_2, \ldots$ for quark masses, and $M_1, M_2, \ldots$ for hadron masses.

nates the leading effect of a mistuned chromomagnetic coupling c_B.

A better approach, still using a hadron's kinetic mass, is as follows. Reference [48] analyzes the Breit equation to show how higher-order potentials and the p^4 terms generate B_2, tracing how the mismatches noted in Eqs. (2.29) and (2.30) propagate to B_2. This analysis reveals that the discretization error in B_2 is smaller for heavy-light hadrons than for quarkonium states. For heavy-light hadrons, the largest part of the kinetic binding energy comes from the light quarks and gluons, and, since the light quark has mass $ma \ll 1$, its contribution to the kinetic binding energy of the meson has only a small discretization error. To tune κ for charmed and bottom quarks, it is therefore better to use heavy-light states, such as $D_s^{(*)}$ and $B_s^{(*)}$, whose kinetic masses have the smallest statistical, discretization, and chiral extrapolation errors. In fact, the leading discretization error, from the chromomagnetic energy, can again be removed by taking the spin-averaged mass of the pseudoscalar and vector mesons.

It is sometimes thought that the tuning inaccuracy of the kinetic binding energy B_2 can be circumvented by adjusting ζ so that (a hadron's) $M_1 = M_2$, and then fixing M_1 to experiment. But any discretization error in B_2 is then propagated to ζ and, hence, throughout the rest of the simulation. It is, therefore, just as clean to leave $\zeta = 1$ and tune M_2 to a target meson mass, as we have done here.

At this stage, it may be helpful to compare and contrast the Fermilab approach [5,47] with lattice NRQCD [3,4]. The construction of lattice NRQCD starts with the (dimensionally regulated and $\overline{\text{MS}}$-renormalized) NRQCD effective Lagrangian for continuum QCD [42,43], and then discretizes it. This process can be repeated order-by-order in perturbation theory. In the Fermilab method, a version of the Wilson-Sheikholeslami-Wohlert lattice action is used, but the results are interpreted with (dimensionally regulated and $\overline{\text{MS}}$-renormalized) NRQCD with modified short-distance coefficients. This is possible because Wilson fermions possess heavy-quark symmetry, and the proposed improvements preserve this feature. Then the parallel structure of the NRQCD descriptions of QCD and lattice gauge theory are used to match the latter to the former. In both frameworks, the lattice action can be systematically improved via the nonrelativistic expansion [4,47].

At a practical level, early spectrum calculations [49] use a lattice-NRQCD action [4] that adjusts, at the tree level, the full v^4 Lagrangian and the spin-dependent v^6 Lagrangian.[2] The p^4 terms are, thus, correctly normalized at the tree level, so the quarkonium and heavy-light kinetic mass tunings are comparably accurate. On the other hand, the Fermilab action has tree-level errors in the v^6 and even some of the v^4 terms. The errors diminish monotonically as a is reduced, however. This is especially important for charmonium: here the nonrelativistic expansion is not especially good, but it is needed only to organize the matching of the most important couplings in S, knowing that further errors, such as those described by $\mathcal{L}_{\text{HQ}}^{(6)}$, are of the form $(mv^2a)^2$ and smaller.

In summary, the pattern of discretization effects leads us to tune κ via kinetic masses corresponding to the $\overline{1S}$, D_s, and B_s mesons. The main spectroscopic results, presented in Sec. IV, are for mass splittings, in which case the uncertainties are minimized by quoting differences of our computed rest masses.

D. Correlator construction

The meson correlator at a given spatial momentum $\boldsymbol{p}$ and time t is defined as

$$C_{ab}(\boldsymbol{p}, t) = \sum_{\boldsymbol{x}} e^{-i\boldsymbol{p}\cdot\boldsymbol{x}} \langle 0|O_a(\boldsymbol{x}, t) O_b^\dagger(\boldsymbol{0}, 0)|0\rangle, \tag{2.33}$$

where $\boldsymbol{x}$ is the spatial coordinate. The source and sink meson operators O_b and O_a have the form

$$O_c(\boldsymbol{x}, t) = \sum_{\boldsymbol{y}} \bar{\psi}(\boldsymbol{x}, t) \Gamma \phi_c(\boldsymbol{x} - \boldsymbol{y}) \psi(\boldsymbol{y}, t), \tag{2.34}$$

where Γ is a product of Dirac matrices appropriate for the meson spin structure, and $\phi_c(\boldsymbol{x} - \boldsymbol{y})$ is a smearing function. Neglecting the disconnected piece, the meson correlator can be rewritten with the quark propagators

$$G(\boldsymbol{x}, t; \boldsymbol{0}, 0) = \int [d\psi][d\bar{\psi}] \psi(\boldsymbol{x}, t) \bar{\psi}(\boldsymbol{0}, 0) e^{-S}, \tag{2.35}$$

with S from Eq. (2.6), yielding

$$C_{ab}(\boldsymbol{p}, t) = \sum_{\boldsymbol{x}} e^{-i\boldsymbol{p}\cdot\boldsymbol{x}} \times \text{Tr}[G(\boldsymbol{0}, 0; \boldsymbol{x}, t) \Gamma G_{ab}(\boldsymbol{x}, t; \boldsymbol{0}, 0) \Gamma^\dagger], \tag{2.36}$$

where

$$G_{ab}(\boldsymbol{x}, t; \boldsymbol{0}, 0) = \sum_{\boldsymbol{y}, \boldsymbol{z}} \phi_a(\boldsymbol{x} - \boldsymbol{y}) G(\boldsymbol{y}, t; \boldsymbol{z}, 0) \phi_b^\dagger(\boldsymbol{z}) \tag{2.37}$$

is the smeared quark propagator.

For the P states, we use two types of quarkonium correlators, which we call "relativistic" and "nonrelativistic." In the relativistic case, all four spin components of the quark propagators were used to construct the two-point functions. We used point and smeared sources and sinks. The smearing functions $\phi_c(\boldsymbol{x})$ are $1S$ and $2S$ wave functions of the QCD-motivated Richardson potential [50]. At the sink, spatial momentum $\boldsymbol{p} = 2\pi(n_1, n_2, n_3)/L$ is given to the quarkonium state. We restrict the range of $\boldsymbol{p}$ such that $\sum n_i^2 \leq 9$. Using this approach, we computed correlation functions for the $1S$ and $2S$ states for the pseudoscalar and the vector to study both the kinetic and rest masses. For

[2]The HPQCD Collaboration's most recently published unquenched calculations [19] of the bottomonium spectrum with lattice NRQCD are obtained from an action without the spin-dependent v^6 corrections.

the $1P$ states h, χ_0, and χ_1 we computed only the rest masses.

In the nonrelativistic approach to constructing the two-point functions, the meson operators project onto two of the Dirac components of the quark fields. Table II gives the explicit form of these operators. At the source and sink we smear the quark propagators with a P-type wave function $\phi_c(\boldsymbol{r}) = \phi_{1S}(|\boldsymbol{r}|)\hat{r}_i$, where $\phi_{1S}(|\boldsymbol{r}|)$ is a Richardson $1S$ wave function [50] and $i = 1, 2, 3$. At the origin we set $\phi_c(\boldsymbol{0}) = 0$. The relativistic interpolating operators include extra lower Dirac components that increase the overlap with excited states. Therefore, one should expect that the overlap of the nonrelativistic meson operators with the $1P$ ground states would be better than in the relativistic case. We used these nonrelativistic operators at $\boldsymbol{p} = \boldsymbol{0}$ for the h, χ_0, χ_1, and χ_2 states. In Sec. III A, we compare the results for the first three states with the corresponding results from relativistic operators.

For both correlator constructions, we use several time-slice positions for the source vectors. In the case of the coarse $\beta = 6.76$, $am_l/am_s = 0.005/0.05$ ensemble and all medium-coarse ensembles, we use eight sources for the relativistic operators; in all other cases, we use four.

E. Fitting methods

To determine the mass spectrum, we fit our correlator data with a Bayesian procedure, taking priors guided by potential models [50,51]. The priors, listed in Table III, are the same for both relativistic and nonrelativistic correlators. To find the quarkonium masses from relativistic correlators, we use a delta function and a $1S$ smearing wave function as the source and sink. We fit simultaneously two or three source-sink combinations for the zero-momentum states, including the ground state and up to two excited states. The minimum and maximum source-sink separation is varied, and the best fit is selected based on the confidence level and the size of the errors in the ground state and first excited-state masses. After choosing the fit range, 250 bootstrap samples are generated to provide an error estimate.

The fitting method in the case of nonrelativistic operators is similar except we use the same P-type wave function, described above, for both source and sink. In this case, we use no more than a ground state plus one excited state in the fitting form. The quality of data in the nonrelativistic case is such that often a fit with just the ground state is enough, provided the fitting range is appropriately chosen.

TABLE II. Nonrelativistic meson operators for the $1P$ states. The smearing operator in spatial direction i is denoted by p_i. The indices j and k are different from i and each other, and repeated indices on the last line are not summed over.

Meson	$^{2S+1}L_J$	Irrep.	Operator	
h	$^1P_1$	T_1	p_i,	$i = 1, 2, 3$
χ_0	$^3P_0$	A_1	$\sum_{i=1}^{3} \sigma_i p_i$	
χ_1	$^3P_1$	T_1	$\sigma_j \times p_k$,	$i = 1, 2, 3$
χ_2	$^3P_2$	T_2	$\sigma_j p_k + \sigma_k p_j$,	$i = 1, 2, 3$
χ_2	$^3P_2$	E_2	$\sigma_j p_j - \sigma_k p_k$,	$i = 1, 2$

TABLE III. Prior central values for the ground-state masses. The priors' widths are all fixed to 0.5.

a (fm)	κ	$M_{q\bar{q}}a$
≈ 0.18	0.120	1.932 386
≈ 0.15	0.122	1.841 549
	0.076	3.818 718
≈ 0.12	0.122	1.539 279
	0.086	3.187 431
≈ 0.09	0.127	1.184 840
	0.0923	2.818 421

III. GENERAL RESULTS

Before presenting results for mass splittings (in Sec. IV) we discuss three general issues: a comparison of the statistical quality of relativistic and nonrelativistic operators (Sec. III A); a numerical comparison of tuning κ via M_2 in heavy-light and quarkonium (Sec. III B); and a discussion of how uncertainties from tuning κ are propagated to the mass splitting (Sec. III C).

A. Relativistic vs nonrelativistic operators

The statistical quality of our data can be judged from Fig. 1, which shows examples of typical two-point functions for the $1S$ pseudoscalar and vector states and their corresponding effective masses, calculated with relativistic operators. The data are from the coarse ensemble with $am_l/am_s = 0.01/0.05$. We have a clear signal and the effective masses have well-established plateaus. As already mentioned, for the $1P$ states we used both relativistic and nonrelativistic types of operators. Figure 2 compares the effective masses of the $h_c(1P)$ and $h_b(1P)$ states, calculated with both types of operators. The data show that the effective masses obtained with nonrelativistic operators plateau at an earlier t_{min}. Despite the fact that the statistics in the nonrelativistic case are, in this example, 3 times lower than in the relativistic case, the errors on the fitted h_c and h_b masses are smaller than the ones calculated with relativistic operators. This finding holds for all of the $1P$ states studied here. Our statistics with the nonrelativistic operators are 2–3 times lower than with the relativistic ones (except for the medium-coarse case where they are 6 times lower), yet the errors on the masses are up to 50% smaller, and in some cases smaller still—see Tables IV, V, VI, and VII for numerical comparisons. The nonrelativistic operators couple much more weakly to the excited states and, thus, yield effective mass plateaus of better quality and fitted masses with smaller errors. All of our results for

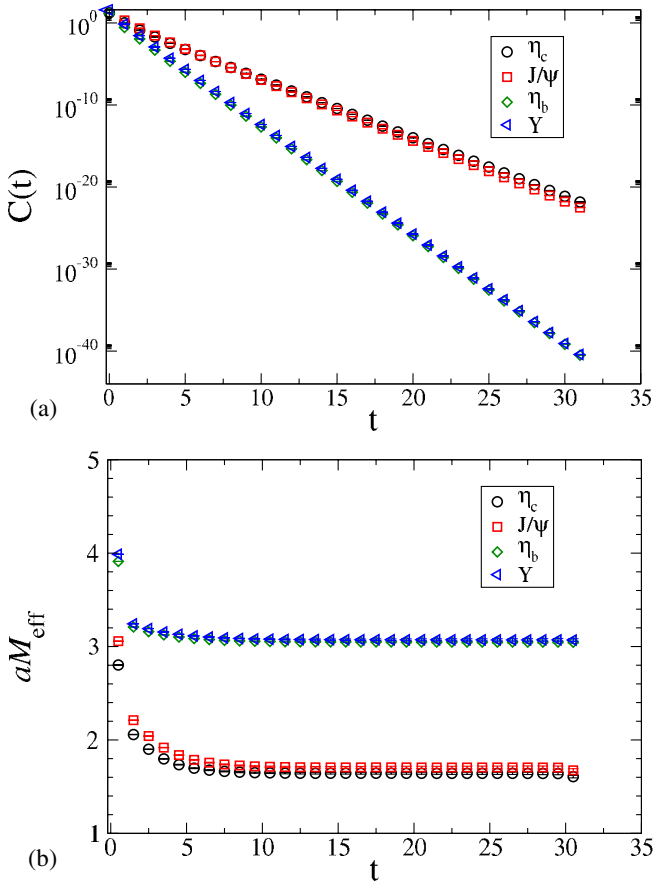

FIG. 1 (color online). Propagators (a) and effective masses (b) for the η_c, J/ψ, η_b, and Υ states, with delta-function sources and sinks, from the coarse ensemble with $am_l/am_s = 0.01/0.05$.

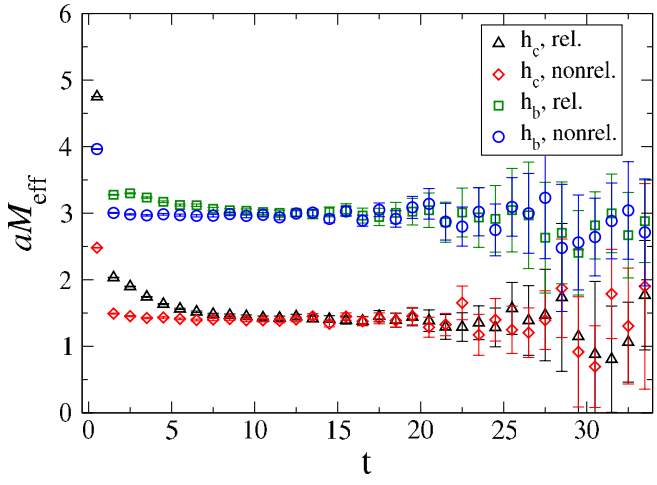

FIG. 2 (color online). Comparison between effective masses for h_c and h_b calculated with relativistic and nonrelativistic operators, on the fine ensemble with $am_l/am_s = 0.0124/0.031$.

quarkonium masses are listed in Tables IV, V, VI, and VII with statistical errors calculated with the bootstrap method and symmetrized.

The central values of the $1P$ states calculated with relativistic and nonrelativistic operators occasionally differ by more than 1.5 uncorrelated σ. This difference arises more often than expected, especially once correlations are considered. In the tables, these cases are labeled with a star. To check whether this difference is due to statistics, in some cases we carried out simultaneous fits to both the relativistic and nonrelativistic correlators. The masses extracted this way turned out to be indistinguishable from the masses from nonrelativistic data alone. This was not surprising, because the data from relativistic sources had larger fluctuations than that from nonrelativistic sources. Thus, in our further analysis of the chiral extrapolation and a dependence, we use the nonrelativistic results for the $1P$ states wherever they are available.

B. κ tuning in quarkonium and heavy-strange mesons

In Sec. II C, we argued that the best way to tune the hopping parameter κ is to use the spin-averaged kinetic mass of heavy-strange hadrons. If instead one would tune to the kinetic mass of the (spin-averaged) quarkonium ground state, the resulting tuned κ could be different at nonzero lattice spacing. To study this discrepancy we have computed the quarkonium $\overline{1S}$ kinetic mass for a wide range of κ on the medium-coarse ensemble with $am_l/am_s = 0.0290/0.0484$. Figure 3 shows the results and also shows the physical $aM(\overline{1S})$ and aM_Υ.[3] From a polynomial fit to the data, we get $\kappa_c \approx 0.122$ for the charmed quark, which is the same value as the one we obtain from matching to D_s. However, because the relevant discretization effects are larger in bottomonium than in B mesons, the tuned values of the hopping parameter differ substantially: $\kappa_b \approx 0.094$ from Υ vs $\kappa_b \approx 0.076$ from B_s.

When we tune to the D_s, some uncertainty in κ arises. We take the tuning error in κ_c to be 0.0015 and in κ_b to be 0.006. Reference [9] finds uncertainties (statistical and fitting) in this range on the medium-coarse, coarse, and fine ensembles, and here we assume the same for the extra-coarse ensembles. We discuss in the next subsection how to propagate these errors to our computed splittings.

Above we mentioned a small difference in tuning the clover coupling for the coarse ensembles. The value of the tadpole coefficient u_0 used in that analysis was determined from mean Landau gauge link whereas the coefficient used in the others was determined from the plaquette. This difference means that our bare quark mass, i.e. κ, has a slightly different definition on the coarse ensembles. Discrepancies in mass splittings caused by this choice should be eliminated via the nonperturbative tuning.

[3]When this tuning was carried out, the η_b had not yet been observed by experiment.

TABLE IV. Rest masses of the charmonium states η_c, J/ψ, h_c χ_{c0}, and χ_{c1} calculated with relativistic operators. All masses in units of $r_1 = 0.318$ fm. The star denotes masses that differ from their counterparts in Table V by more than 1.5σ.

a (fm)	β	κ_c	$\eta_c(1^1S_0)$	$\eta_c(2^1S_0)$	$J/\psi(1^3S_1)$	$\psi(2^3S_1)$	$h_c(1^1P_1)$	$\chi_{c0}(1^3P_0)$	$\chi_{c1}(1^3P_1)$
≈ 0.18	6.503	0.120	3.2924(9)	4.24(6)	3.4452(16)	4.35(7)	4.185(17)	⋆4.079(12)	⋆4.052(89)
	6.485	0.120	3.3071(14)	4.42(4)	3.4581(18)	4.48(3)	4.214(26)	4.117(15)	⋆4.173(13)
	6.467	0.120	3.3327(7)	4.39(27)	3.4862(11)	4.45(11)	4.213(29)	4.109(12)	4.200(25)
	6.458	0.120	3.3481(13)	4.47(6)	3.5004(16)	4.43(10)	⋆4.217(18)	4.106(18)	⋆4.181(19)
≈ 0.15	6.586	0.122	3.5688(8)	4.66(3)	3.7317(13)	4.75(3)	⋆4.476(8)	4.341(6)	4.450(7)
	6.572	0.122	3.5883(9)	4.64(5)	3.7501(14)	4.79(2)	⋆4.495(8)	4.368(6)	4.471(17)
≈ 0.12	6.81	0.122	3.8721(11)	5.16(4)	4.0594(18)	5.25(3)	4.807(17)	4.626(10)	4.755(19)
	6.79	0.122	3.8876(12)	5.14(3)	4.0747(18)	5.22(4)	4.821(12)	4.657(10)	4.791(10)
	6.76, a	0.122	3.8824(9)	5.09(4)	4.0677(15)	5.10(5)	4.800(13)	4.658(8)	4.758(15)
	6.76, b	0.122	3.9009(8)	5.12(3)	4.0864(11)	5.27(3)	4.817(14)	4.650(30)	4.785(15)
≈ 0.09	7.11	0.127	4.2740(26)	5.33(13)	4.4460(22)	5.55(6)	5.159(29)	5.027(16)	5.185(10)
	7.09	0.127	4.2885(15)	5.52(4)	4.4596(15)	5.66(4)	⋆5.149(24)	⋆4.986(15)	⋆5.123(19)
	7.08	0.127	4.2889(26)	5.51(5)	4.4613(33)	5.65(7)	5.167(33)	⋆4.986(26)	5.133(48)

TABLE V. Rest masses of the charmonium states h_c, χ_{c0}, χ_{c1}, and χ_{c2} calculated with nonrelativistic operators. All masses in units of $r_1 = 0.318$ fm. The star denotes masses that differ from their counterparts in Table IV by more than 1.5σ.

a (fm)	β	κ_c	$h_c(1^1P_1)$	$\chi_{c0}(1^3P_0)$	$\chi_{c1}(1^3P_1)$	$\chi_{c2}(1^3P_2)$
≈ 0.18	6.503	0.120	4.213(1)	⋆4.111(9)	⋆4.210(9)	4.272(15)
	6.485	0.120	4.227(7)	4.105(8)	⋆4.200(7)	4.286(10)
	6.467	0.120	4.223(12)	4.127(7)	4.227(8)	4.278(15)
	6.458	0.120	⋆4.253(9)	4.128(9)	⋆4.222(9)	4.310(11)
≈ 0.15	6.600	0.122	4.492(7)	4.344(6)	4.458(7)	4.537(11)
	6.586	0.122	⋆4.493(7)	4.349(7)	4.462(7)	4.536(13)
	6.572	0.122	⋆4.516(9)	4.375(9)	4.488(9)	4.574(10)
	6.566	0.122	4.548(10)	4.405(6)	4.526(7)	4.614(10)
≈ 0.09	7.11	0.127	5.199(11)	5.030(8)	5.170(12)	5.257(12)
	7.09	0.127	⋆5.198(13)	⋆5.034(11)	⋆5.168(13)	5.257(14)
	7.08	0.127	5.178(15)	⋆5.047(8)	5.167(13)	5.232(18)

C. κ-tuning uncertainties

Tables IV, V, VI, and VII and most of the plots in Sec. IV show statistical errors only, because the foremost aim of this paper is to understand the pattern of discretization errors. A systematic error also arises from inaccuracies in tuning κ_c and κ_b, and to study the continuum limit it is necessary to propagate this error to the mass splittings. We discuss here how we treat these uncertainties.

TABLE VI. Rest masses of the bottomonium states η_b, Υ, h_b, χ_{b0}, and χ_{b1} calculated with relativistic operators. All masses in units of $r_1 = 0.318$ fm. The star denotes masses that differ from their counterparts in Table VII by more than 1.5σ.

a (fm)	β	κ_b	$\eta_b(1^1S_0)$	$\eta_b(2^1S_0)$	$\Upsilon(1^3S_1)$	$\Upsilon(2^3S_1)$	$h_b(1^1P_1)$	$\chi_{b0}(1^3P_0)$	$\chi_{b1}(1^3P_1)$
≈ 0.15	6.586	0.076	7.3776(8)	8.202(5)	7.4100(9)	8.209(5)	8.269(120)	⋆8.162(35)	⋆8.147(40)
	6.572	0.076	7.4061(9)	8.241(63)	7.4386(9)	8.248(7)	8.321(13)	8.292(11)	8.318(11)
≈ 0.12	6.81	0.086	8.0690(10)	8.933(12)	8.1299(12)	8.957(12)	8.919(15)	8.855(13)	8.898(13)
	6.79	0.086	8.0563(17)	8.910(14)	8.1167(19)	8.929(14)	8.902(19)	8.850(21)	8.874(38)
	6.76, a	0.086	7.9815(9)	8.870(11)	8.0426(13)	8.890(10)	8.860(20)	8.796(13)	8.839(14)
≈ 0.09	7.11	0.0923	10.2040(15)	11.130(78)	10.2627(19)	11.160(32)	11.050(14)	⋆11.006(13)	⋆11.049(10)
	7.09	0.0923	10.1861(11)	11.142(20)	10.2468(15)	11.161(18)	⋆11.056(19)	10.992(14)	11.034(13)
	7.08	0.0923	10.1795(26)	11.112(30)	10.2397(33)	11.137(56)	⋆11.066(19)	⋆11.017(12)	⋆11.048(14)

TABLE VII. Rest masses of the charmonium states h_b, χ_{b0}, χ_{b1}, and χ_{b2} calculated with nonrelativistic operators. All masses in units of $r_1 = 0.318$ fm. The star denotes masses that differ from their counterparts in Table VI by more than 1.5σ.

a (fm)	β	κ_b	$h_b(1^1P_1)$	$\chi_{b0}(1^3P_0)$	$\chi_{b1}(1^3P_1)$	$\chi_{b2}(1^3P_2)$
≈ 0.15	6.600	0.076	8.254(8)	8.220(8)	8.243(8)	8.274(9)
	6.586	0.076	8.252(10)	⋆8.216(10)	⋆8.242(10)	8.276(10)
	6.572	0.076	8.321(11)	8.288(10)	8.312(11)	8.341(11)
	6.566	0.076	8.369(9)	8.335(9)	8.359(9)	8.391(10)
≈ 0.09	7.11	0.0923	11.046(9)	⋆10.981(10)	⋆11.022(11)	11.077(8)
	7.09	0.0923	⋆11.020(10)	10.973(10)	11.006(12)	11.040(10)
	7.08	0.0923	⋆11.014(10)	⋆10.964(11)	⋆11.008(10)	11.045(9)

Several pieces of evidence show that the spin-averaged splittings depend very little on κ. These splittings vary little from charmonium to bottomonium [24], a feature understood to be a consequence of both systems lying between the confining and Coulombic part of the potential [1,2]. This feature is, in fact, reproduced in our lattice-QCD data. Moreover, earlier work in the quenched approximation [52] and with $n_f = 2$ [8] show negligible κ dependence for spin-averaged splittings. Thus, we shall assume that the κ-tuning error for these splittings can be neglected.

For spin-dependent splittings, we compute the $1S$ hyperfine splitting as a function of κ, on the medium-coarse ensemble with $am_l/am_s = 0.0290/0.0484$, the same ensemble as in Fig. 3. The data are summarized in Table VIII. We fit the data to the form

$$\mu = 1/\kappa - 1/\kappa_{\rm cr}, \tag{3.1}$$

$$\text{HFS} = b_0/\mu^2 + b_1/\mu^3 + b_2/\mu^4 + b_3/\mu^5 + b_4/\mu^6, \tag{3.2}$$

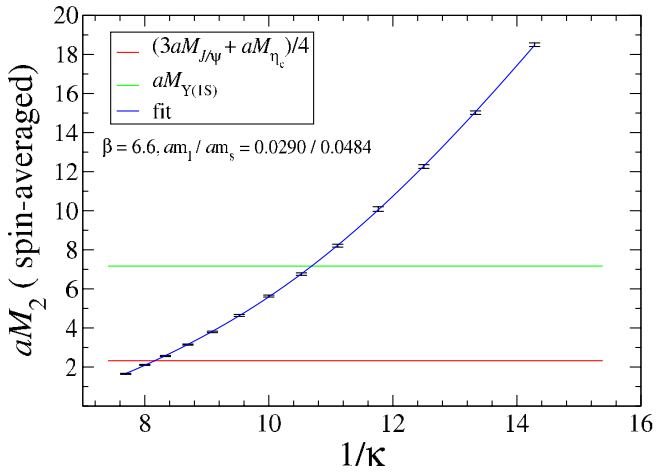

FIG. 3 (color online). Spin-averaged kinetic mass aM_2 as a function of κ, over a wide range, on the medium-coarse ensemble with $am_l/am_s = 0.0290/0.0484$. With a polynomial fit to the data, we can read off $\frac{1}{4}(aM_{\eta_c} + 3aM_{J/\psi})$ and aM_Υ, finding $\kappa_c \approx 0.122$ and $\kappa_b \approx 0.094$.

for $\kappa_{\rm cr} = 0.145$, which enforces the requirement that, at large heavy-quark mass $m_0 = \mu/2a$, the splitting goes as $1/m_0^2$. The fit gives $\chi^2/\text{dof} = 0.6/8$, where dof is degrees of freedom. From the fit result we estimate that an error of 0.0015 in the determination of κ_c results in a 6% error in the charmonium hyperfine splitting, and an error of 0.006 in the determination of κ_b, a 22% error in the bottomonium hyperfine splitting. We expect that these errors are characteristic of all splittings driven by the spin-spin and tensor terms in the quarkonium effective potential, since in the nonrelativistic treatment, they all stem from the same term in the heavy-quark effective Lagrangian.

The spin-orbit splitting remains to be considered. In our data and in experiment, it decreases from charmonium to bottomonium similarly to the hyperfine and tensor splittings. Therefore, we shall assume the same relative error from the uncertainty in tuning κ.

Below we also present results for the splittings between twice the spin-averaged mass of D_s and D_s^*, and of B_s and B_s^*, and the corresponding $\overline{1S}$ quarkonium mass. To estimate their κ-tuning errors we have calculated these spin-averaged masses for several values of κ near κ_c and κ_b on the coarse ensemble with $am_l/am_s = 0.01/0.05$. These

TABLE VIII. 1^3S_1-1^1S_0hyperfine splittings in r_1 units as a function of the valence κ calculated for the medium-coarse ensemble with $am_l/am_s = 0.0290/0.0484$.

κ	$r_1[M(1^3S_1) - M(1^1S_0)]$
0.070	0.0247(9)
0.075	0.0299(11)
0.080	0.0369(12)
0.085	0.0442(13)
0.090	0.0531(14)
0.095	0.0631(15)
0.100	0.0749(17)
0.105	0.0885(18)
0.110	0.1029(23)
0.115	0.1244(27)
0.120	0.1499(33)
0.125	0.1836(40)
0.130	0.2335(49)

direct measurements allow us to propagate the κ-tuning errors from the masses to the mass splittings. We obtain an error of 1.3% for charm and 13% for bottom. We assume the same error for these splittings at other lattice spacings.

IV. SPECTRUM RESULTS

We now present plots of quarkonium mass splittings as a function of the square of the sea-quark pion mass. The splittings and their errors are calculated using the bootstrap method. In most cases, we expect the dependence on the sea-quark mass to be mild, so we perform on our results a chiral extrapolation linear in M_π^2 down to the physical pion. The extrapolated values are denoted in each plot with filled symbols. The error bars come from symmetrizing the 1σ (68%) interval of the bootstrap distribution.

Where possible, we compare our results to experimental measurements. As a rule we take the average values from the compilation of the Particle Data Group [24]. The exception is the mass of the $\eta_b(1S)$ meson, which has only recently been observed. We take $M_{\eta_b} = 9390.9 \pm 2.8$ MeV, based on our average of two measurements by the *BABAR* Collaboration [53,54] and one by the CLEO Collaboration [55].

In examining the results, we are interested in seeing how well we can understand discretization errors via the nonrelativistic description of Eqs. (2.13), (2.14), and (2.15). We therefore carry out separate chiral extrapolations at each lattice spacing, and discuss whether the a dependence, and any deviations from experiment, make sense.

From the effective Lagrangian discussion, we expect different discretization errors to affect spin-averaged and spin-dependent splittings. Errors in the spin-averaged splittings stem from the Darwin ($\boldsymbol{D}\cdot\boldsymbol{E}$) term and the two p^4 terms. Errors in the spin-dependent splittings stem from the chromomagnetic ($i\boldsymbol{\sigma}\cdot\boldsymbol{B}$) and spin-orbit ($i\boldsymbol{\sigma}\cdot\boldsymbol{D}\times\boldsymbol{E}$) terms. Moreover, from the general structure of potentials arising from QCD [25,26], we learn that $i\boldsymbol{\sigma}\cdot\boldsymbol{B}$ predominantly affects $M(nS_{\rm HFS})$ and $M(nP_{\rm tensor})$, while $i\boldsymbol{\sigma}\cdot\boldsymbol{D}\times\boldsymbol{E}$ affects $M(nP_{\text{spin-orbit}})$.

A. Spin-averaged splittings

Let us start with $\overline{1P}$-$\overline{1S}$ and 1^1P_1-$\overline{1S}$ splittings, plotted in Figs. 4 and 5 vs $(r_1M_\pi)^2$. In the nonrelativistic picture, they arise predominantly at order v^2 via the kinetic energy, which our tuning of κ should normalize correctly. The spin-dependent terms in $\mathcal{L}^{(4)}_{\rm HQ}$ [cf. Eq. (2.15)] do not contribute to spin averages ($\overline{1S}$, $\overline{1P}$) or to a spin singlet (1^1P_1). Discretization errors remain, however, at order v^4 via the mismatches in Eqs. (2.28), (2.29), and (2.30). We assess these results using the error estimates in Ref. [47], which account for both the a dependence and the relative v^2 suppression.

Our results for charmonium are shown in Fig. 4. Our results for both splittings approach the continuum physical point as the lattice spacing decreases, and the size of the discretization effects is about what one expects: 5–6% from $m_E \neq m_2$ and 3–6% from $m_4 \neq m_2$ [47].

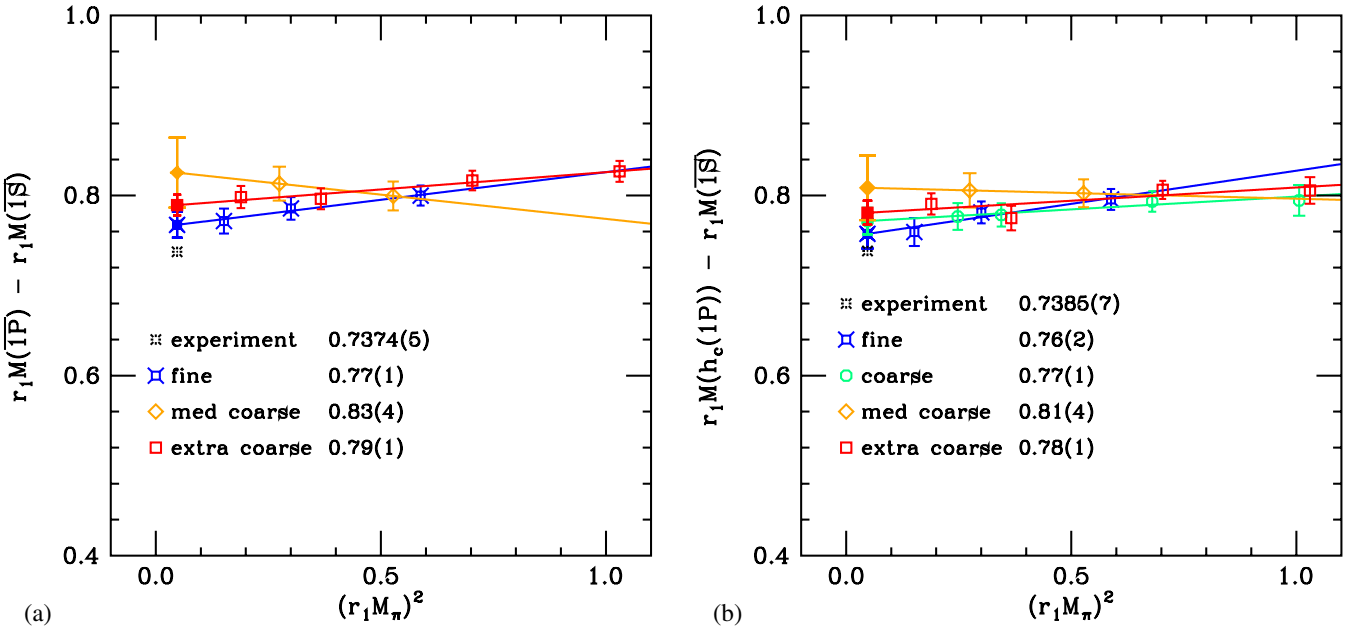

FIG. 4 (color online). The (a) $\overline{1P}$-$\overline{1S}$ and (b) 1^1P_1-$\overline{1S}$ splittings in charmonium. The fine ensemble data are in blue fancy squares, the coarse in green circles, the medium-coarse in orange diamonds and the extra-coarse in red squares. The chirally extrapolated values are given in the legend and plotted with filled symbols.

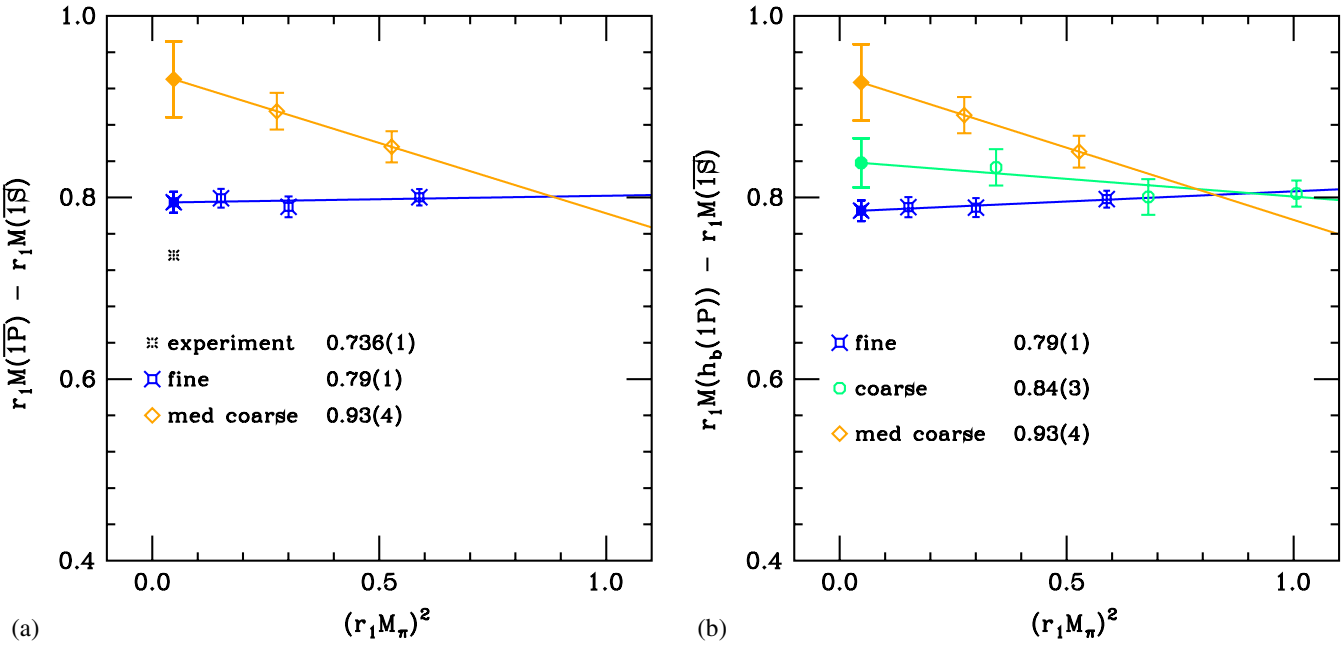

FIG. 5 (color online). The (a) $\overline{1P}$-$\overline{1S}$ and (b) 1^1P_1-$\overline{1S}$ splittings in bottomonium. Color and symbol code as in Fig. 4.

The $\overline{1P}$-$\overline{1S}$ and 1^1P_1-$\overline{1S}$ splittings in bottomonium are given in Fig. 5. These splittings agree acceptably with experiment, given the estimated discretization errors, 2–3% from $m_E \neq m_2$ and 2–5% from $m_4 \neq m_2$ [47]. We cannot compare the $h_b(1^1P_1)$ mass with experiment, because that state has not been observed [24], but our results for the 1^1P_1 level agree very well with the $\overline{1^3P_J}$ average.

Next let us examine the $\overline{2S}$-$\overline{1S}$ splitting. We fit a correlator matrix constructed from two interpolating operators, local and smeared, to three or more states (i.e., two or more excited states). The error we assign to the mass determination estimates the uncertainties in our method. The results for charmonium as a function of $(r_1M_\pi)^2$ are shown in Fig. 6(a). The lattice data appear to lie significantly

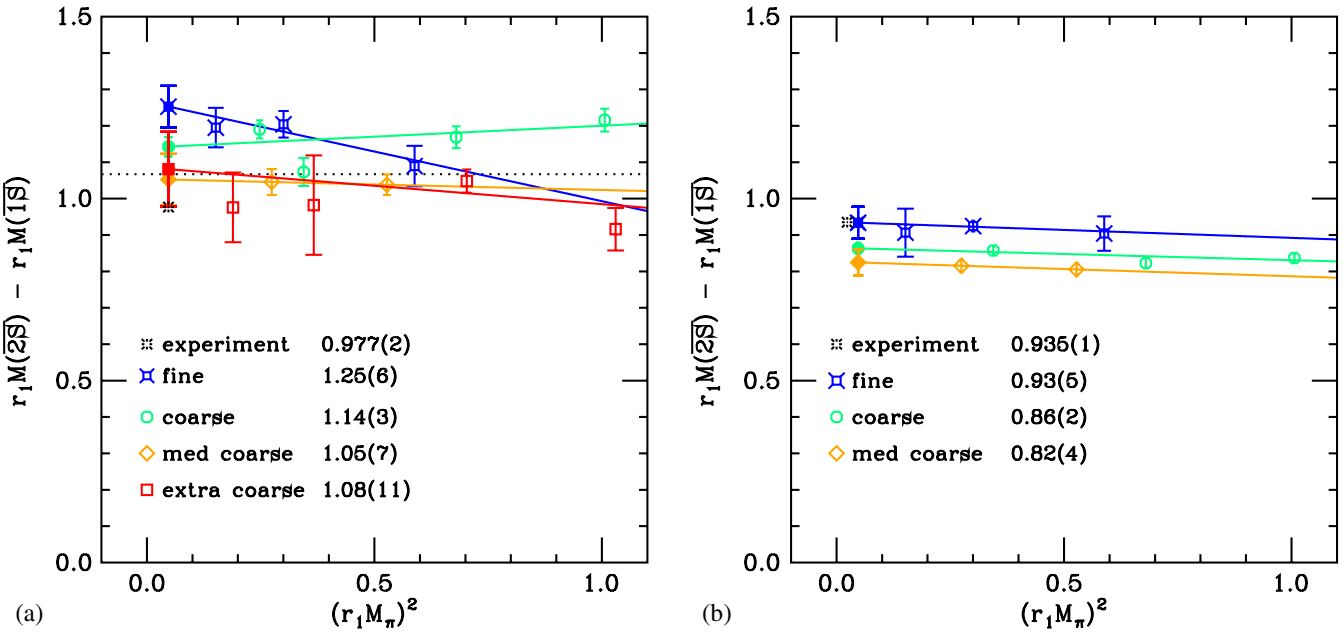

FIG. 6 (color online). Splitting between the $\overline{2S}$ and $\overline{1S}$ levels of (a) charmonium and (b) bottomonium. The dotted line in (a) indicates the open-charm threshold. The experimental point in (b) is *not* the spin-averaged splitting, but the $\Upsilon(2S)$-$\overline{1S}$ mass difference, since the η_b' has not been observed.

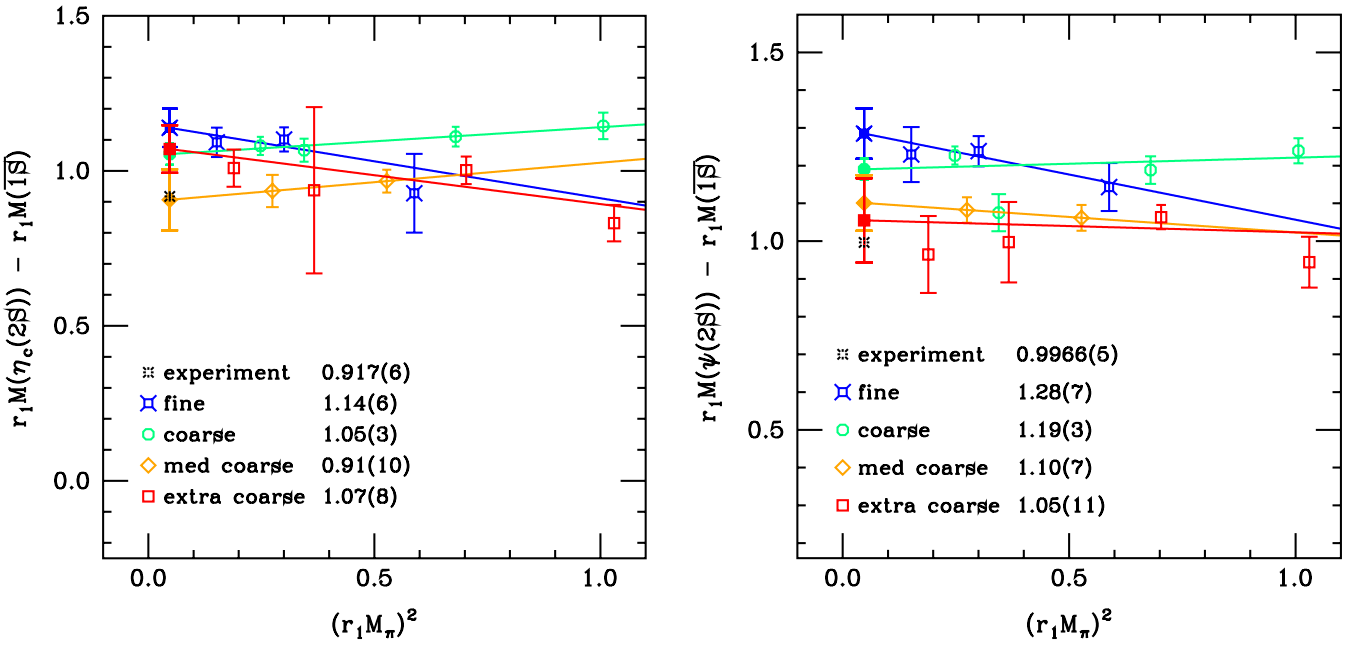

FIG. 7 (color online). Splittings in charmonium between the individual $2S$ states and the $\overline{1S}$ level.

above the experimental value at the smaller lattice spacings. The individual $2S$ levels show the same trends we observe in the spin-averaged level. In Fig. 7 we plot separately the $\eta_c(2S)$-$\overline{1S}$ and $\psi(2S)$-$\overline{1S}$. We see that both $\eta_c(2S)$ and $\psi(2S)$ are responsible for the behavior seen in Fig. 6(a), the latter especially so. The results for bottomonium (Fig. 6(b)) are more satisfactory.

We suggest two possible reasons for the behavior of the charmonium $\overline{2S}$-$\overline{1S}$ splitting results. First, the $2S$ are the only excited states in this study. Excited states are more difficult than ground states to determine accurately. With only two operators, our fits are less reliable, even though our fit model has at least three states. Second, the fit procedure does not take into account adequately the possible contribution of multiple open-charm levels. For example, we have not used a two-body operator in the matrix correlator. With unphysically large quark masses, the open-charm levels are unphysically high. As the sea-quark mass

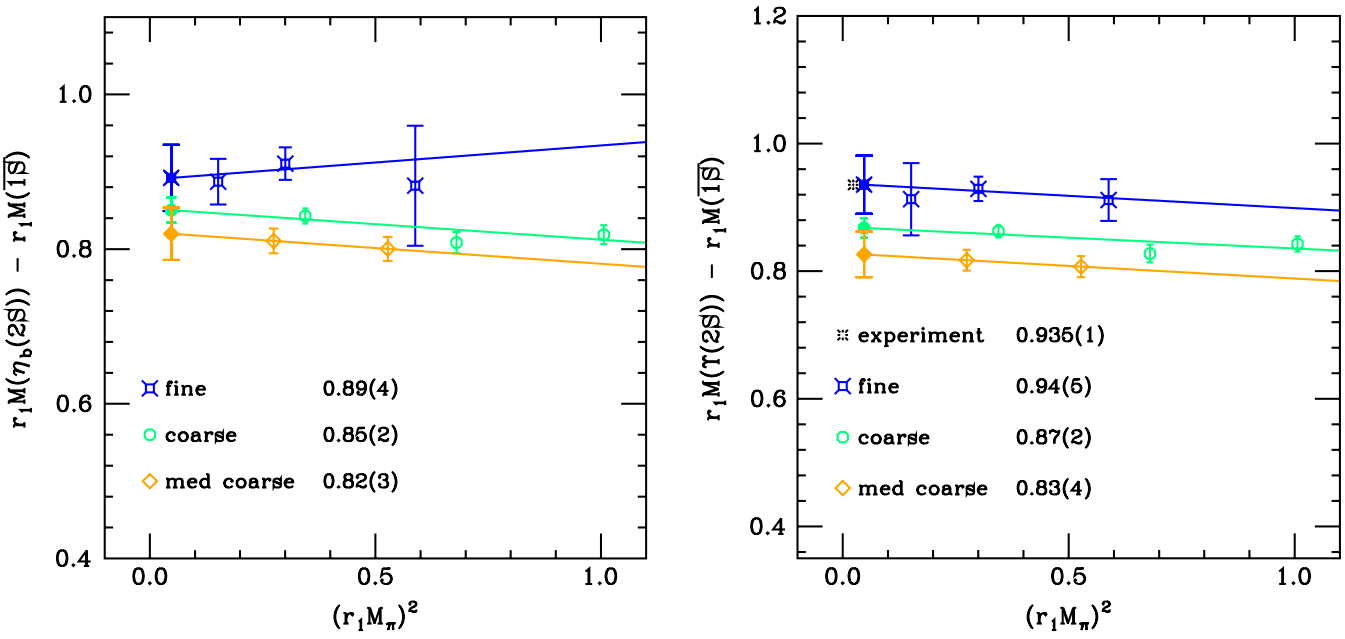

FIG. 8 (color online). Splittings in bottomonium between the individual $2S$ states and the $\overline{1S}$ level.

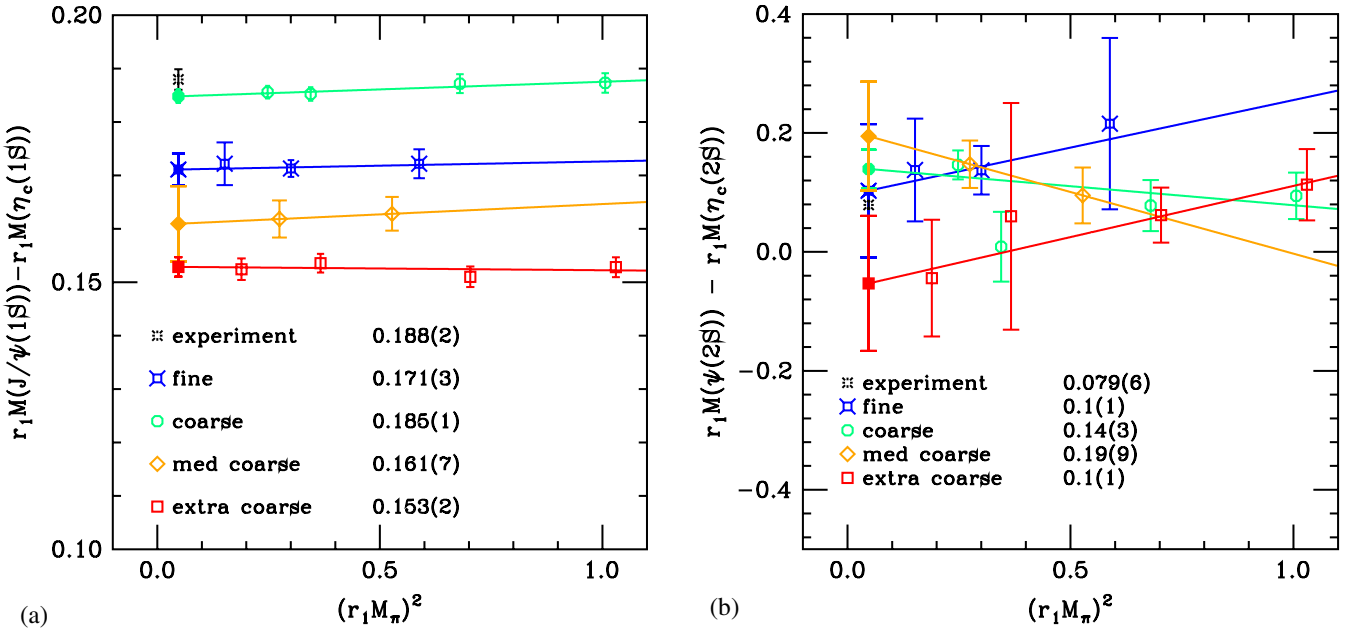

FIG. 9 (color online). Charmonium hyperfine splittings for (a) $1S$ and (b) $2S$.

is decreased, they come down. Moreover, the box size of our lattices at the lightest sea-quark mass is larger, which decreases the discrete level spacing of the would-be open-charm continuum. The dotted line in Fig. 6(a) shows the location of the physical open-charm threshold. It is dangerously close to the physical $2S$ levels, especially the $\psi(2S)$. Thus it is conceivable that nearby multiple open-charm levels are being confused with the $2S$ and artificially raise its fitted mass. This explanation is consistent with the observed gradual rise of this level in the fine ensembles with decreasing light quark mass but not with the trends seen in the coarse and medium-coarse ensembles.

For bottomonium in Fig. 6(b), the open bottom threshold is safely distant (off scale in this plot), so we do not expect a similar confusion in this channel. Figure 8 shows the individual $2S$ bottomonium levels separately. There is no comparison for the first excited pseudoscalar state $\eta_b(2S) - \overline{1S}$, because the state has not yet been observed [24], although the extrapolated values appear to approach a consistent continuum limit. The first excited vector state splitting $\Upsilon(2S)$-$\overline{1S}$ is given in Fig. 8(b). The chirally extrapolated values monotonically approach the experimental value and for the fine ensembles our splitting agrees with the experiment.

B. Hyperfine splittings

Now let us turn to the hyperfine structure. Our results for the hyperfine splitting in charmonium and bottomonium are presented in Figs. 9 and 10. For the $1S$ levels and for $2S$ bottomonium, there is little dependence on the sea-quark mass. To assess the approach to the continuum limit one must bear in mind that the errors in Figs. 9 and 10 are statistical only, and the systematic error from κ tuning must also be taken into account. We thus take the values at the physical pion mass, apply the κ-tuning error and plot these data vs a^2, as shown in Fig. 11. Both data sets are consistently linear in a^2, so we carry out such an extrapolation. The extrapolated values in units of r_1 are 0.187(12) for charmonium, with $\chi^2/\mathrm{dof} = 1.9/2$, and 0.087(20) for bottomonium, with $\chi^2/\mathrm{dof} = 0.55/1$. One can see, from comparing Fig. 11 with Fig. 9 and 10, that the κ-tuning uncertainties inherited from the heavy-strange kinetic mass are larger than the statistical uncertainties of the quarkonium rest-mass splittings.

In physical units these extrapolated results are $M_{J/\psi(1S)} - M_{\eta_c(1S)} = 116.0 \pm 7.4^{+2.6}_{-0.0}$ MeV and $M_{\Upsilon(1S)} - M_{\eta_b(1S)} = 54.0 \pm 12.4^{+1.2}_{-0.0}$ MeV, where the second error comes from converting from r_1 units to MeV. For charmonium the average of experimental measurements is 116.4 ± 1.2 MeV [24], so our result is perfectly consistent. For bottomonium, the experimental measurements are $71.4^{+2.3}_{-3.1} \pm 2.7$ MeV [53], $66.1^{+4.9}_{-4.8} \pm 2.0$ MeV [54], and $68.5 \pm 6.6 \pm 2.0$ MeV [55]; symmetrizing the error bars and taking a weighted average, we find $M_{\Upsilon(1S)} - M_{\eta_b(1S)} = 69.4 \pm 2.8$ MeV. Our hyperfine splitting thus falls 1.2σ short. Note that with lattice NRQCD, the HPQCD Collaboration finds $M_{\Upsilon(1S)} - M_{\eta_b(1S)} = 61 \pm 4 \pm 13$ MeV [19], which agrees with the recent experimental measurements, yet also with our result.

The errors on the final $1S$ hyperfine splittings quoted here encompass statistics (as amplified by extrapolations), κ tuning, and r_1. In addition, the coupling c_B has been adjusted only at the tree level, introducing an error of $O(\alpha_s a)$ that our continuum extrapolation would not elimi-

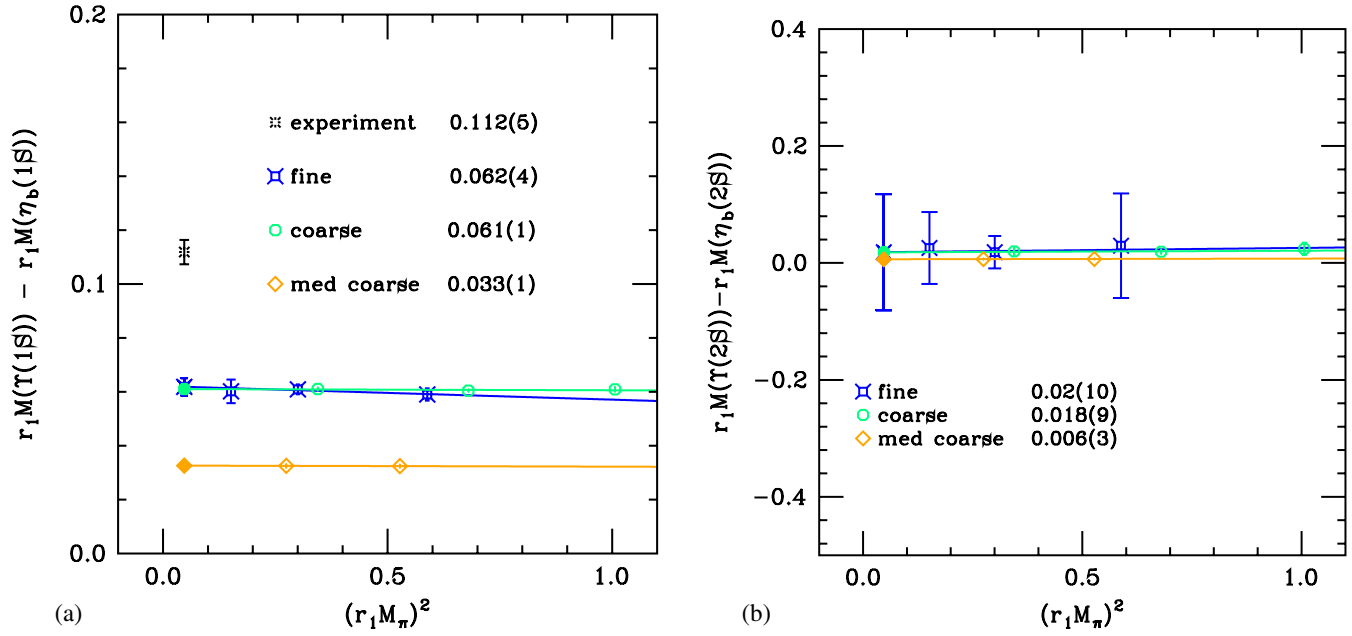

FIG. 10 (color online). Bottomonium hyperfine splittings for (a) $1S$ and (b) $2S$.

nate. A preliminary result for the one-loop correction to c_B is available [56], suggesting that a very small correction is needed beyond the tadpole improvement of Eq. (2.26), when u_0 is set from the Landau link.

The $2S$ hyperfine splittings for both charmonium and bottomonium are shown in Figs. 9(b) and 10(b). Unfortunately, these results are not very useful. Although the charmonium splitting agrees, within large errors, with experiment, one should bear in mind the issue of threshold effects surrounding our determination of the $\psi(2S)$ mass, discussed above. The bottomonium splitting does not suffer from this problem, but the statistical and fitting errors are still too large to make a prediction of the as yet unobserved $\eta_b(2S)$ mass.

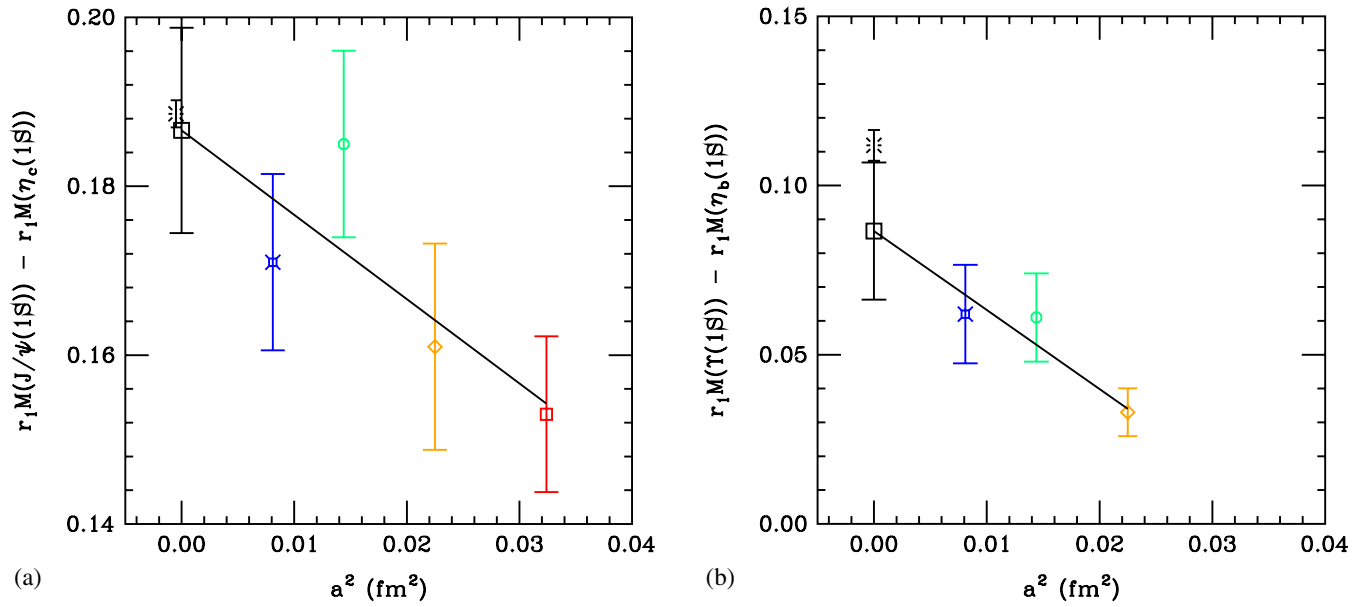

FIG. 11 (color online). Continuum extrapolations for the $1S$ hyperfine splittings for (a) charmonium and (b) bottomonium. The symbols and colors of the data points are the same as throughout the paper. Here the error bars on the data points include our estimates for the κ-tuning systematic error. The plotted experimental η_b mass comes from the average of recent measurements [53–55], as discussed in the text.

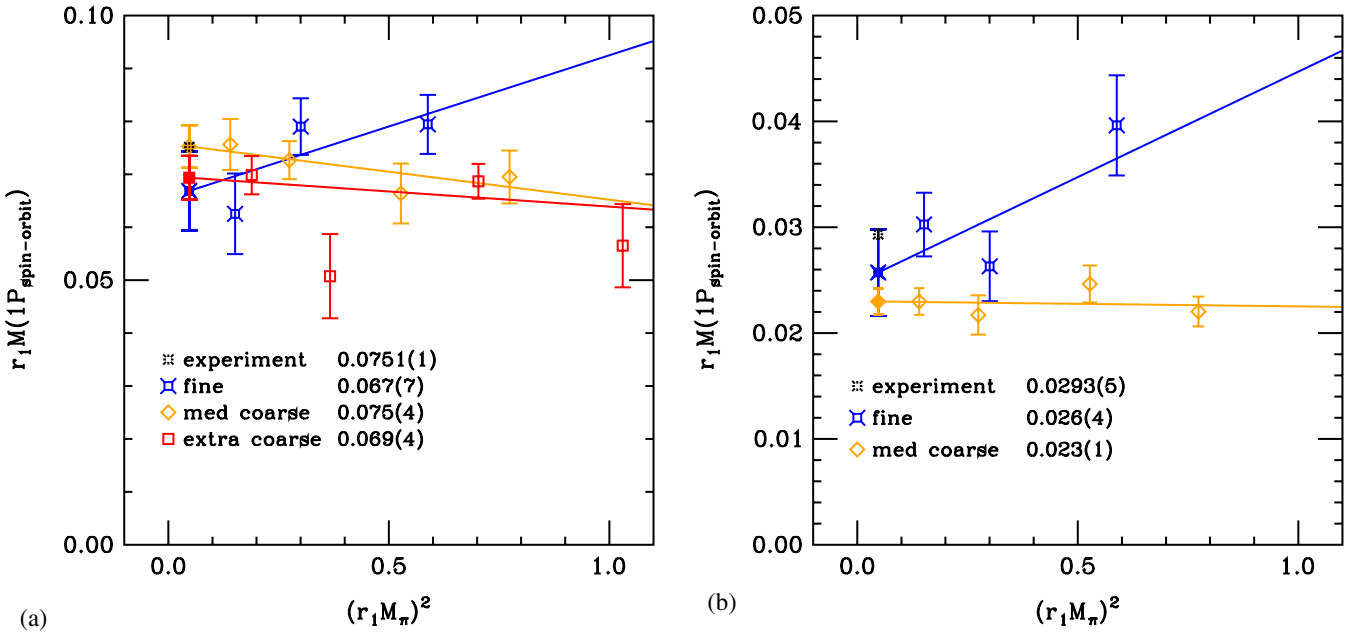

FIG. 12 (color online). Spin-orbit splittings in $1P$ levels, with $M(1P_{\text{spin-orbit}})$ defined in Eq. (2.4), for (a) charmonium and (b) bottomonium.

C. *P*-state splittings

We now turn to splittings between the 1^3P_J levels, which stem from two contributions [25]. As discussed above, one comes from exchanging a Coulomb gluon between a spin-orbit term, $\bar{h}^{(\pm)}i\boldsymbol{\sigma}\cdot(\boldsymbol{D}\times\boldsymbol{E})h^{(\pm)}$ in Eq. (2.15), and the static potential, $\bar{h}^{(\mp)}A_4h^{(\mp)}$. The other comes from exchanging a transverse gluon between the chromomagnetic terms, $\bar{h}^{(+)}i\boldsymbol{\sigma}\cdot\boldsymbol{B}h^{(+)}$ and $\bar{h}^{(-)}i\boldsymbol{\sigma}\cdot\boldsymbol{B}h^{(-)}$. These two contributions can be separated by forming the combinations in Eqs. (2.4) and (2.5) [26].

The spin-orbit splittings $M(1P_{\text{spin-orbit}})$ are shown in Fig. 12 for charmonium and bottomonium. They exhibit a small lattice-spacing dependence and agree well with experiment, indicating that the chromoelectric interactions and, hence, c_E are adjusted accurately enough. The tensor splittings $M(1P_{\text{tensor}})$ are shown in Fig. 13 for charmonium and bottomonium. These chromomagnetic effects seem to

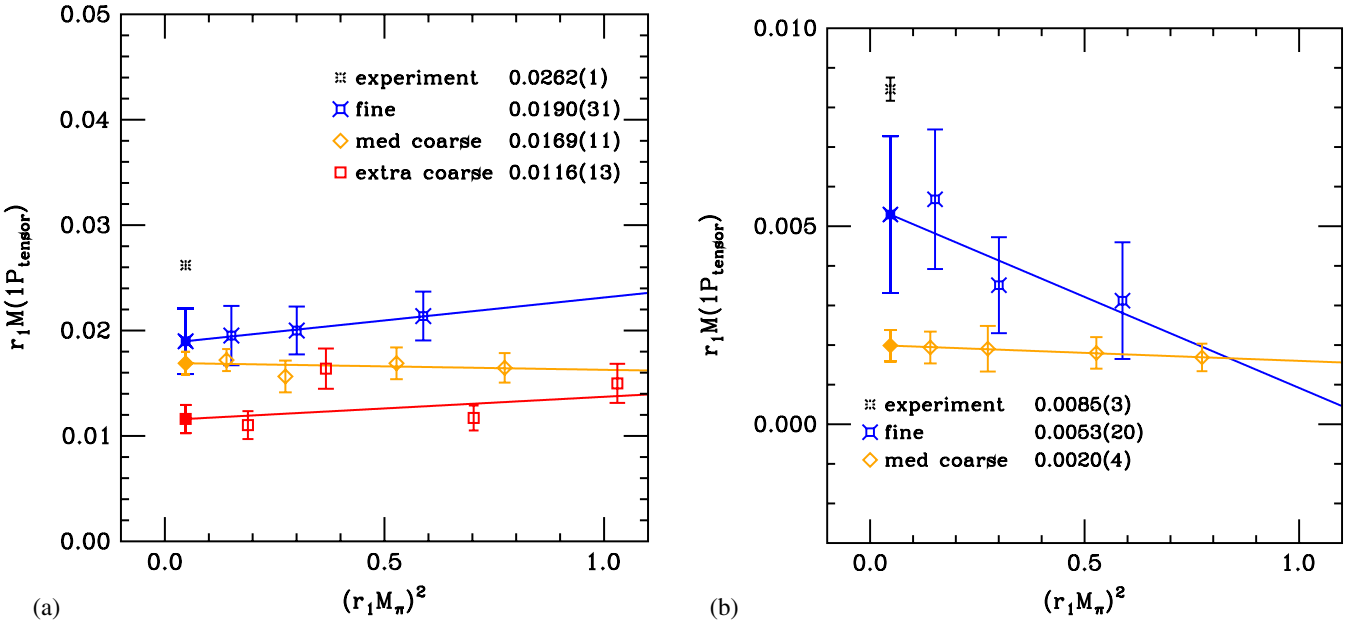

FIG. 13 (color online). Tensor splittings in $1P$ levels, with $M(1P_{\text{tensor}})$ defined in Eq. (2.5), for (a) charmonium and (b) bottomonium.

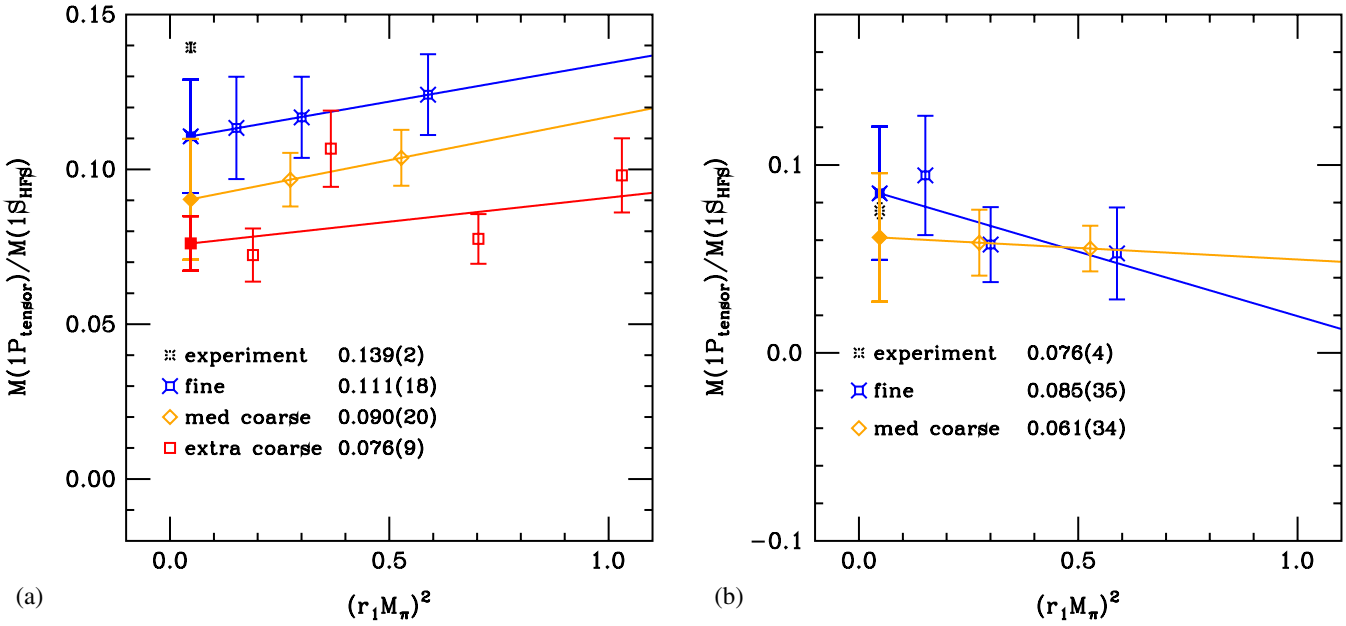

FIG. 14 (color online). Ratio of the $1P$ tensor and $1S$ hyperfine splittings, for (a) charmonium and (b) bottomonium.

approach the experimental value as a decreases. Since the tensor and the spin-spin potential components both measure the effects of the chromomagnetic interaction, we plot the ratio of the $1P$ tensor splitting to the $1S$ hyperfine splitting in Fig. 14. The coefficient m_B^{-1} should drop out from the ratio and if there are no effects from higher-dimension operators, the ratio should be a constant which agrees with the continuum limit. If a higher-dimension operator has a significant contribution, then the ratio need not agree any better than the splittings themselves. The charmonium case, Fig. 14(a), seems to suggest that the higher-dimension operator matters, the bottomonium case, Fig. 14(b), seems to suggest it does not. This outcome is plausible, because the v^2 suppression of the higher-dimension operator is 10% in bottomonium, but only 30% in charmonium [cf. Eqs. (2.11) and (2.12)].

D. Quarkonium vs heavy-strange mesons

Unlike other approaches to heavy quarks, lattice QCD is supposed to treat heavy-light mesons and quarkonium on the same footing. If we form the splitting

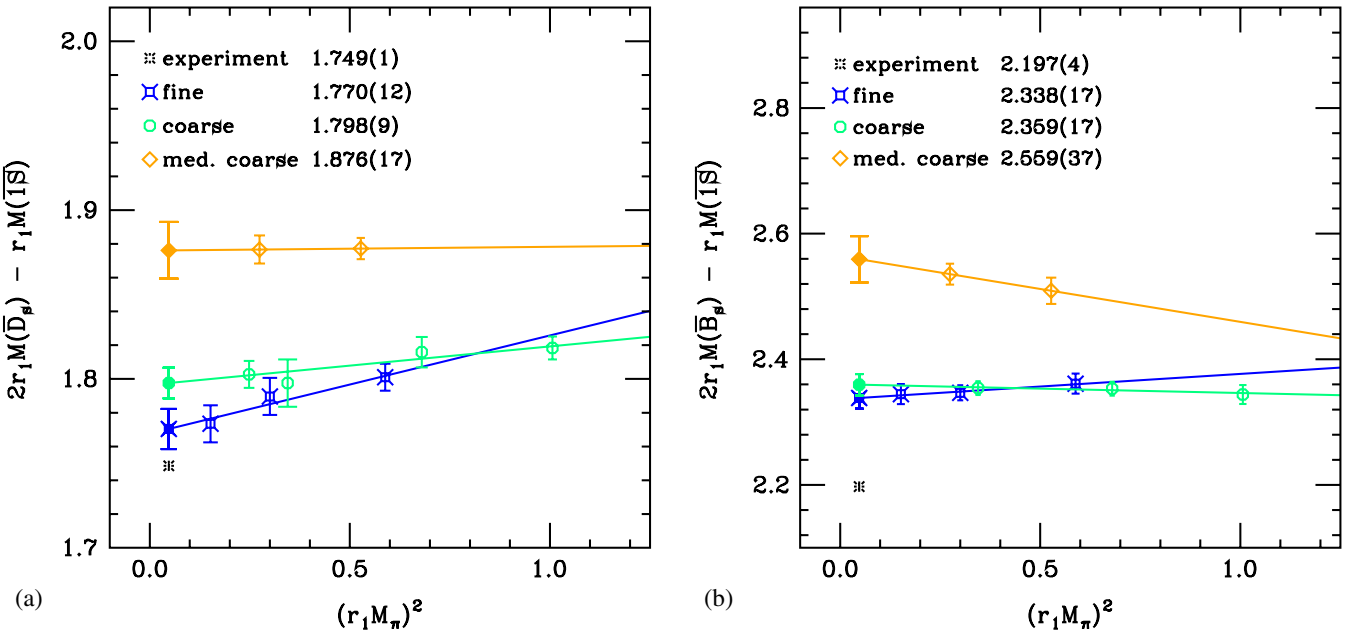

FIG. 15 (color online). Quarkonium–heavy-light splittings (a) $2M(\bar{D}_s) - M(\overline{1S})$ and (b) $2M(\bar{B}_s) - M(\overline{1S})$.

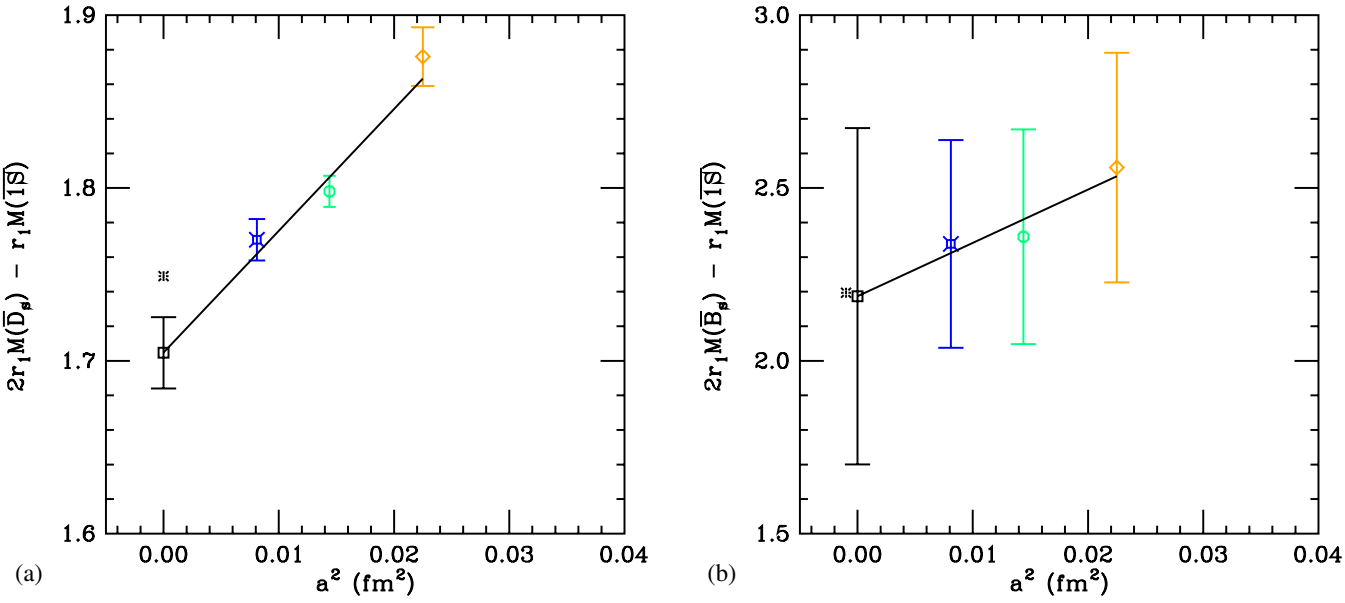

FIG. 16 (color online). Continuum extrapolations of (a) $2M(\bar{D}_s) - M(\overline{1S})$ and (b) $2M(\bar{B}_s) - M(\overline{1S})$.

$$2M(\bar{D}_s) - M(\overline{1S}) \tag{4.1}$$

the rest mass drops out, leaving a pure QCD quantity. Here $M(\bar{D}_s)$ denotes the spin average of D_s and D_s^* masses. This mass difference is interesting from the point of view of the discretization effects, which should contribute less to the $\bar{D}_s$ and $\bar{B}_s$ than to the charmonium and bottomonium $\overline{1S}$ states. We show this splitting (also for the bottom-quark sector) combining our quarkonium rest masses with the Fermilab-MILC heavy-strange rest masses [9] in Fig. 15. The correlation in the error is treated correctly with the bootstrap method and, as elsewhere in this paper, the bootstrap errors are symmetrized. Clearly, discretization effects are important at nonzero a.

In Fig. 16, we incorporate the κ-tuning errors and show the a dependence of the above splittings. Carrying out an extrapolation linear in a^2, which is empirically suitable, we find $r_1[2M(\bar{D}_s) - M(\overline{1S})] = 1.705 \pm 0.021$ and $r_1[2M(\bar{B}_s) - M(\overline{1S})] = 2.19 \pm 0.49$; these correspond to $2M(\bar{D}_s) - M(\overline{1S}) = 1058 \pm 13^{+24}_{-0}$ MeV and $2M(\bar{B}_s) - M(\overline{1S}) = 1359 \pm 304^{+31}_{-0}$ MeV, with the uncertainty in r_1 yielding the second error bar. The bottomonium extrapolation agrees with the experimental value, but the combined statistical and κ-tuning errors are quite large. The charmonium extrapolation is 1σ shy of the experimental value. Given the empirical nature of our continuum extrapolation, this is completely satisfactory.

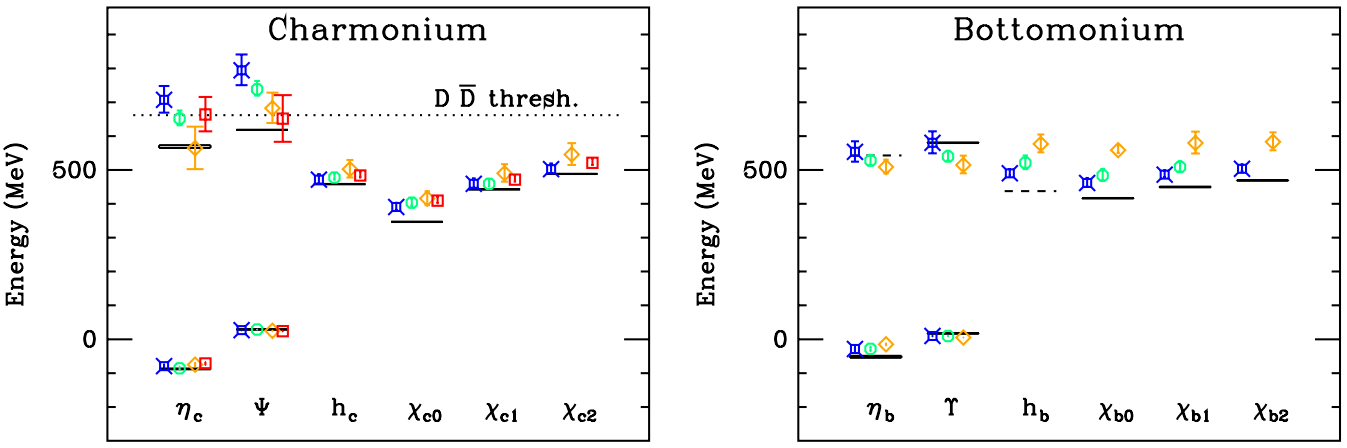

FIG. 17 (color online). Quarkonium spectrum as splittings from the $\overline{1S}$ level for $\bar{c}c$ (left) and $\bar{b}b$ (right). The fine-ensemble results are in blue fancy squares, the coarse in green circles, the medium-coarse in orange diamonds, and the extra-coarse in red squares. Solid lines show the experimental values, and dashed lines estimates from potential models. The dotted line in the left panel indicates the physical open-charm threshold. The error on the data points combines statistical, κ-tuning, and r_1 uncertainties.

TABLE IX. Continuum extrapolations of splittings in charmonium and bottomonium in MeV. The first error comes from statistics and accumulated extrapolation systematics; the second comes from the uncertainty in scale setting with $r_1 = 0.318^{+0.000}_{-0.007}$ fm.

Splitting	Charmonium		Bottomonium	
	This work	Experiment	This work	Experiment
$\overline{1P}$-$\overline{1S}$	$473 \pm 12^{+10}_{-0}$	457.5 ± 0.3	$446 \pm 18^{+10}_{-0}$	456.9 ± 0.8
$^1P_1$-$\overline{1S}$	$469 \pm 11^{+10}_{-0}$	457.9 ± 0.4	$440 \pm 17^{+10}_{-0}$	...
$\overline{2S}$-$\overline{1S}$	$792 \pm 42^{+17}_{-0}$	606 ± 1	$599 \pm 36^{+13}_{-0}$	(580.3 ± 0.8)[a]
1^3S_1-1^1S_0	$116.0 \pm 7.4^{+2.6}_{-0}$	116.4 ± 1.2	$54.0 \pm 12.4^{+1.2}_{-0}$	69.4 ± 2.8
$1P$ tensor	$15.0 \pm 2.3^{+0.3}_{-0}$	16.25 ± 0.07	$4.5 \pm 2.2^{+0.1}_{-0}$	5.25 ± 0.13
$1P$ spin-orbit	$43.3 \pm 6.6^{+1.0}_{-0}$	46.61 ± 0.09	$16.9 \pm 7.0^{+0.4}_{-0}$	18.2 ± 0.2
$1S$ $\bar{s}Q$-$\bar{Q}Q$	$1058 \pm 13^{+24}_{-0}$	1084.8 ± 0.8	$1359 \pm 304^{+31}_{-0}$	1363.3 ± 2.2

[a]$\Upsilon(2S)$-$\overline{1S}$ instead of $\overline{2S}$-$\overline{1S}$.

E. Summary of spectrum results

To summarize our results, Fig. 17 shows the charmonium and the bottomonium spectra as splittings from the $\overline{1S}$ level and compares them to the experimental results. We have plotted the chirally extrapolated values at each lattice spacing and included statistical, κ-tuning, and r_1 uncertainties. Solid lines show the experimental values, where they are known, and dashed lines show estimates from potential models [51] in other cases.

For the splittings discussed above, Table IX shows the continuum limit, taken via linear extrapolations in a^2. One should bear in mind that the NRQCD-based theory of cutoff effects, explained in Sec. II C, anticipates a less trivial lattice-spacing dependence. The linear-in-a^2 extrapolations are consistent with the data, which are not yet sufficient to resolve more complicated functional forms. In Table IX the second (asymmetric) error bar comes from the conversion to MeV with $r_1 = 0.318^{+0}_{-0.007}$ fm $= 1.611^{+0}_{-0.035}$ GeV^{-1} [33–35].

The charmonium and bottomonium spectra by and large show good agreement with experiment. The charmonium hyperfine splitting agrees very well; the bottomonium splitting agrees at 1.2σ. The tensor and spin-orbit splittings also agree well, for both systems. The $^1P_1$-$\overline{1S}$ and $\overline{1P}$-$\overline{1S}$ spin-averaged splittings agree at 1.1–1.3σ for $\bar{c}c$; the $\overline{1P}$-$\overline{1S}$ at 0.6σ for $\bar{b}b$. As discussed above, the charmonium $2S$ states are too high, because our operator basis and statistics proved to be insufficient to disentangle the bound states from open-charm threshold effects. For bottomonium the $\overline{2S}$-$\overline{1S}$ splitting does not suffer from threshold effects and agrees well. When the r_1 uncertainty is included, the splitting of quarkonium relative to the heavy-strange spectrum, $2M(\bar{D}_s) - M(\overline{1S})$ and $2M(\bar{B}_s) - M(\overline{1S})$, also agrees well with experiment.

V. CONCLUSIONS

Quarkonium properties offer an excellent test of lattice QCD, because they are relatively well-understood hadrons, via potential models and effective field theories. This paper attempts a thorough study of the charmonium and bottomonium mass splittings, using lattice gauge fields with $2 + 1$ flavors of sea quarks. By using the Fermilab method for heavy quarks, we are able to study both systems, as well as heavy-light hadrons, with the same basic theoretical tool. By using the MILC ensembles, we are able to study a wide range of lattice spacing, and a wide range of up and down sea-quark masses, down to $0.10m_s$.

Our aim here has been to develop methods and to compare discretization effects against expectations that are gleaned from an effective theory analysis. An important technical finding for ground P states is that nonrelativistic operators are superior to relativistic operators in overlap and, hence, statistics.

Our calculations reproduce most features of the mass splittings, to the extent expected. This optimistic conclusion is marred somewhat, because we find that the errors from κ tuning are significant for spin-dependent splittings. Agreement with experiment is found only when these uncertainties, which stem from the heavy-strange kinetic mass, are taken in to account. In some other cases, such as leptonic decay constants for heavy-light mesons [11], uncertainties in κ also influence significantly the final error budget.

In the continuation of this project, we hope to improve on the results presented here in several ways. First, the MILC ensembles now contain approximately 4 times as many configurations, and they extend to smaller lattice spacings, $a \approx 0.06$ fm and $a \approx 0.045$ fm. The finer lattice will bring charm into the region where Symanzik-motivated continuum extrapolations are justified and should bring bottomonium discretization effects under 1%. To this end it may also prove worthwhile to incorporate the p^4 corrections of the improved Fermilab action [47]. Higher statistics and twisted-boundary conditions [57] should improve the tuning of κ and, thus, reduce errors from this source as well.

ACKNOWLEDGMENTS

Computations for this work were carried out on facilities of the USQCD Collaboration, which are funded by the Office of Science of the U.S. Department of Energy. This

work was supported in part by the U.S. Department of Energy under Grants No. DE-FC02-06ER41446 (T. B., C. D., L. L.), No. DE-FG02-91ER40661 (S. G.), No. DE-FG02-91ER40677 (A. X. K.), No. DE-FG02-91ER40628 (E. D. F.); by the National Science Foundation under Grants No. PHY-0555243, No. PHY-0757333, No. PHY-0703296 (T. B., C. D., L. L.), and No. PHY-0555235 (E. D. F.); and with support from American Physical Society (E. D. F.). Fermilab is operated by Fermi Research Alliance, LLC, under Contract No. DE-AC02-07CH11359 with the U.S. Department of Energy.

[1] C. Quigg and J. L. Rosner, Phys. Rep. **56**, 167 (1979).
[2] W. Kwong, J. L. Rosner, and C. Quigg, Annu. Rev. Nucl. Part. Sci. **37**, 325 (1987).
[3] G. P. Lepage and B. A. Thacker, Nucl. Phys. B, Proc. Suppl. **4**, 199 (1988); B. A. Thacker and G. P. Lepage, Phys. Rev. D **43**, 196 (1991).
[4] G. P. Lepage, L. Magnea, C. Nakhleh, U. Magnea, and K. Hornbostel, Phys. Rev. D **46**, 4052 (1992).
[5] A. X. El-Khadra, A. S. Kronfeld, and P. B. Mackenzie, Phys. Rev. D **55**, 3933 (1997).
[6] C. Aubin *et al.* (MILC Collaboration), Phys. Rev. D **70**, 094505 (2004); C. W. Bernard *et al.* (MILC Collaboration), Phys. Rev. D **64**, 054506 (2001).
[7] M. Di Pierro *et al.*, Nucl. Phys. B, Proc. Suppl. **119**, 586 (2003); **129**, 340 (2004); S. Gottlieb *et al.*, Proc. Sci., LAT2005 (2006) 203 [arXiv:hep-lat/0510072]; LAT2006 (2006) 175 [arXiv:0910.0048].
[8] A. X. El-Khadra, S. A. Gottlieb, A. S. Kronfeld, P. B. Mackenzie, and J. N. Simone, Nucl. Phys. B, Proc. Suppl. **83**, 283 (2000).
[9] C. Bernard *et al.* (Fermilab Lattice and MILC Collaborations) (unpublished).
[10] C. Aubin *et al.* (Fermilab Lattice and MILC Collaborations), Phys. Rev. Lett. **94**, 011601 (2005); C. Bernard *et al.* (Fermilab Lattice and MILC Collaborations), Phys. Rev. D **79**, 014506 (2009); J. A. Bailey *et al.* (Fermilab Lattice and MILC Collaborations), Phys. Rev. D **79**, 054507 (2009); C. Bernard *et al.* (Fermilab Lattice and MILC Collaborations), Phys. Rev. D **80**, 034026 (2009).
[11] C. Aubin *et al.* (Fermilab Lattice and MILC Collaborations), Phys. Rev. Lett. **95**, 122002 (2005); C. Bernard *et al.* (Fermilab Lattice and MILC Collaborations), Proc. Sci., LAT2008 (2008) 278 [arXiv:0904.1895]; A. Bazavov *et al.* (Fermilab Lattice and MILC Collaborations), Proc. Sci., LAT2009 (2009) 249.
[12] R. T. Evans *et al.* (Fermilab Lattice and MILC Collaborations), Proc. Sci., LAT2006 (2006) 081; LAT2007 (2007) 354 [arXiv:0710.2880]; LAT2008 (2008) 052.
[13] G. S. Bali, Phys. Rep. **343**, 1 (2001).
[14] J. J. Dudek and R. G. Edwards, Phys. Rev. Lett. **97**, 172001 (2006).
[15] J. J. Dudek, R. G. Edwards, and D. G. Richards, Phys. Rev. D **73**, 074507 (2006); J. J. Dudek, R. Edwards, and C. E. Thomas (Hadron Spectrum Collaboration), Phys. Rev. D **79**, 094504 (2009).
[16] J. J. Dudek, R. G. Edwards, N. Mathur, and D. G. Richards, Phys. Rev. D **77**, 034501 (2008).
[17] S. Meinel, Phys. Rev. D **79**, 094501 (2009).
[18] C. T. H. Davies *et al.* (HPQCD, UKQCD, MILC and Fermilab Lattice Collaborations), Phys. Rev. Lett. **92**, 022001 (2004).
[19] A. Gray *et al.* (HPQCD Collaboration), Phys. Rev. D **72**, 094507 (2005).
[20] E. Follana *et al.* (HPQCD Collaboration and UKQCD Collaboration), Phys. Rev. D **75**, 054502 (2007).
[21] C. McNeile, C. T. H. Davies, E. Follana, K. Hornbostel, G. P. Lepage, and J. Shigemitsu (HPQCD Collaboration), arXiv:0910.2921.
[22] I. F. Allison, C. T. H. Davies, A. Gray, A. S. Kronfeld, P. B. Mackenzie, and J. N. Simone (HPQCD and Fermilab Lattice Collaborations), Phys. Rev. Lett. **94**, 172001 (2005).
[23] E. B. Gregory *et al.* (HPQCD Collaboration), Phys. Rev. Lett. **104**, 022001 (2010).
[24] C. Amsler *et al.* (Particle Data Group), Phys. Lett. B **667**, 1 (2008) and update at http://pdg.lbl.gov/.
[25] E. Eichten and F. Feinberg, Phys. Rev. D **23**, 2724 (1981).
[26] M. E. Peskin, Stanford Linear Accelerator Center Report No. SLAC-PUB-3273, 1983 (unpublished).
[27] S. A. Gottlieb, W. Liu, D. Toussaint, R. L. Renken, and R. L. Sugar, Phys. Rev. D **35**, 2531 (1987).
[28] M. Lüscher and P. Weisz, Phys. Lett. **158B**, 250 (1985); P. Weisz, Nucl. Phys. **B212**, 1 (1983); P. Weisz and R. Wohlert, Nucl. Phys. **B236**, 397 (1984); **B247**, 544(E) (1984); G. Curci, P. Menotti, and G. Paffuti, Phys. Lett. **130B**, 205 (1983); **135B**, 516(E) (1984); M. Lüscher and P. Weisz, Commun. Math. Phys. **97**, 59 (1985); **98**, 433(E) (1985).
[29] K. Orginos and D. Toussaint (MILC Collaboration), Phys. Rev. D **59**, 014501 (1998); J. F. Lagaë and D. K. Sinclair, Phys. Rev. D **59**, 014511 (1998); D. Toussaint and K. Orginos (MILC Collaboration), Nucl. Phys. B, Proc. Suppl. **73**, 909 (1999); G. P. Lepage, Phys. Rev. D **59**, 074502 (1999); K. Orginos, R. Sugar, and D. Toussaint, Nucl. Phys. B, Proc. Suppl. **83**, 878 (2000).
[30] Z. Hao, G. M. von Hippel, R. R. Horgan, Q. J. Mason, and H. D. Trottier, Phys. Rev. D **76**, 034507 (2007).
[31] R. Sommer, Nucl. Phys. **B411**, 839 (1994).
[32] C. W. Bernard *et al.*, Phys. Rev. D **62**, 034503 (2000).
[33] A. Bazavov *et al.*, arXiv:0903.3598 [Rev. Mod. Phys. (to be published)].
[34] A. Bazavov *et al.* (MILC Collaboration), Proc. Sci., CD09 (2009) 007 [arXiv:0910.3618]; LAT2009 (2009) 079

[arXiv:0910.3618].
[35] C. T. H. Davies, E. Follana, I. D. Kendall, G. P. Lepage, and C. McNeile (HPQCD Collaboration), arXiv:0910.1229 [Phys. Rev. D (to be published)].
[36] K. G. Wilson, in *New Phenomena in Subnuclear Physics*, edited by A. Zichichi (Plenum, New York, 1977).
[37] B. Sheikholeslami and R. Wohlert, Nucl. Phys. **B259**, 572 (1985).
[38] B. P. G. Mertens, A. S. Kronfeld, and A. X. El-Khadra, Phys. Rev. D **58**, 034505 (1998).
[39] A. S. Kronfeld, Phys. Rev. D **62**, 014505 (2000).
[40] J. Harada, S. Hashimoto, K.-I. Ishikawa, A. S. Kronfeld, T. Onogi, and N. Yamada, Phys. Rev. D **65**, 094513 (2002); **71**, 019903 (2005).
[41] J. Harada, S. Hashimoto, A. S. Kronfeld, and T. Onogi, Phys. Rev. D **65**, 094514 (2002).
[42] W. E. Caswell and G. P. Lepage, Phys. Lett. **167B**, 437 (1986).
[43] G. T. Bodwin, E. Braaten, and G. P. Lepage, Phys. Rev. D **46**, R1914 (1992).
[44] H. W. Lin and N. Christ, Phys. Rev. D **76**, 074506 (2007).
[45] G. P. Lepage and P. B. Mackenzie, Phys. Rev. D **48**, 2250 (1993).
[46] N. H. Christ, M. Li, and H. W. Lin, Phys. Rev. D **76**, 074505 (2007).
[47] M. B. Oktay and A. S. Kronfeld, Phys. Rev. D **78**, 014504 (2008).
[48] A. S. Kronfeld, Nucl. Phys. B, Proc. Suppl. **53**, 401 (1997).
[49] C. T. H. Davies, K. Hornbostel, A. Langnau, G. P. Lepage, A. Lidsey, J. Shigemitsu, and J. H. Sloan, Phys. Rev. D **50**, 6963 (1994).
[50] J. L. Richardson, Phys. Lett. **82B**, 272 (1979).
[51] W. Buchmüller and S.-H. H. Tye, Phys. Rev. D **24**, 132 (1981).
[52] A. X. El-Khadra, Nucl. Phys. B, Proc. Suppl. **30**, 449 (1993).
[53] B. Aubert *et al.* (*BABAR* Collaboration), Phys. Rev. Lett. **101**, 071801 (2008).
[54] B. Aubert *et al.* (*BABAR* Collaboration), Phys. Rev. Lett. **103**, 161801 (2009).
[55] G. Bonvicini *et al.* (CLEO Collaboration), arXiv:0909.5474.
[56] M. Nobes and H. Trottier, Proc. Sci., LAT2005 (2006) 209 [arXiv:hep-lat/0509128].
[57] P. F. Bedaque, Phys. Lett. B **593**, 82 (2004); C. T. Sachrajda and G. Villadoro, Phys. Lett. B **609**, 73 (2005).